ACS Sustainable Chemistry & Engineering

pubs.acs.org/journal/ascecg

Research Article

COSMO-RS-Guided Selection of DES for the Delignification of Sugar Cane Bagasse Allowing the Integrated Recovery of Holocellulose and Functionalized Lignin

Thamiris F. Souza, Ana M. Ferreira,* Filipe H. B. Sosa,* João A. P. Coutinho, Cecília B. Ferreira, and Guilherme M. D. Ferreira*

Cite This: https://doi.org/10.1021/acssuschemeng.6c00062

Read Online

ACCESS | Metrics & More | Article Recommendations | Supporting Information

ABSTRACT: A major challenge in biomass valorization is achieving selective lignocellulose fractionation under mild and sustainable conditions, enabling the recovery of both holocellulose and lignin. Deep eutectic solvents (DES) offer tunable and greener alternatives to conventional pretreatments. This study aimed to develop a dual-valorization strategy for sugar cane bagasse by combining COSMO-RS-guided DES selection with optimized delignification to simultaneously obtain high-purity holocellulose and functionalized lignin. A total of 47,080 DES combinations were screened, identifying diethylene glycol dimethyl ether:ethanolamine (DGDE:ET), acidified with p-toluenesulfonic acid (PTSA), as the most promising solvent. The performance of the selected DGDE:ET+PTSA system was benchmarked against conventional 3% w v^{-1} NaOH extraction and ET+PTSA solvents, and the recovered holocellulose and lignin fractions were systematically characterized through compositional, elemental, and spectroscopic analyses to elucidate structural differences and assess fractionation efficiency. Response surface methodology enabled optimization under mild conditions (DGDE molar fraction 0.10, 100 °C, 0.03 mol L^{-1} PTSA, 90 min, S/L = 1:10), yielding holocellulose-rich solids containing up to 88.9 ± 2.6% holocellulose for derinded bagasse (SGB), comparable to or better than alkaline pretreatment at less corrosive conditions. The DES was also effective for rind-containing bagasse (SGB-C). Lignin recovered from DES extracts exhibited O/N/S functionalization and achieved complete removal of 2,4-dichlorophenoxyacetic acid at near-neutral pH, outperforming Klason lignin, alkaline lignin, holocellulose, bagasse, and biochars. This dual-stream recovery supports an integrated biorefinery pathway that provides high-purity holocellulose for downstream valorization and chemically functionalized lignin for environmental remediation, contributing to more sustainable and circular biomass utilization.

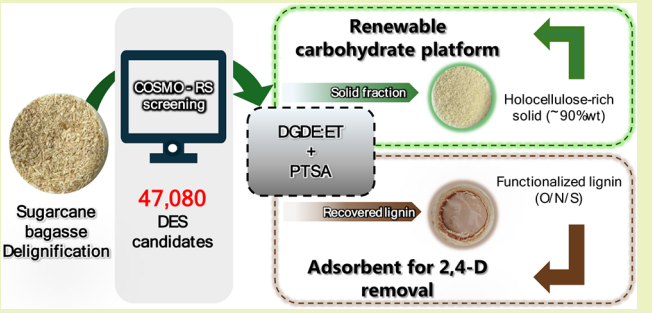

KEYWORDS: *conductor-like screening model for real solvents, lignin precipitation, sustainable biorefinery, diethylene glycol dimethyl ether, ethanolamine*

1. INTRODUCTION

Brazil is the world's largest producer of sugar cane, and the sugar-energy sector plays a central economic role. Processing one ton of sugar cane generates 260−280 kg of bagasse, making it the major residual biomass of the Brazilian agroindustry.[1] With global sugar cane production reaching ~2.0 billion tons in 2023,[2] a large fraction of bagasse remains underexploited. Its valorization is essential to mitigate the environmental impacts associated with lignocellulosic waste while enabling the production of high-value materials.

Sugar cane bagasse is mainly composed of cellulose (~44%), hemicellulose (~28%), and lignin (~21%),[3] and its selective fractionation opens access to applications such as biofuels,[4] insulation materials,[5] cement additives,[6] polymer composites,[7] packaging,[8] and adsorbents.[9] Polysaccharides in particular support high-value applications including biopolymers, nanocomposites,[10] biomedical materials,[11] cosmetic and food ingredients,[12] and biobased platform chemicals,[13] reinforcing the role of integrated biorefineries in exploiting biomass fractions.

Among these fractions, lignin remains underexploited due to its structural complexity, whereas polysaccharides are more readily converted into value-added products. Most solvent-based fractionation studies focus on lignin removal to obtain cellulose- or holocellulose-rich solids, without fully exploring

Received: January 3, 2026
Revised: March 26, 2026
Accepted: March 31, 2026

the potential of the aromatic fraction.[14] Conventional acidic, alkaline, or organic-solvent pretreatments lack selectivity, degrade lignin structures, and compromise their suitability for applications requiring more native features.[15] Nevertheless, lignin exhibits strong potential for adsorption-based remediation, both as biochar[16] and as biosorbent,[17] primarily through aromatic interactions that promote binding of organic contaminants. These insights highlight a largely untapped opportunity to directly valorize lignin-rich streams for environmental remediation without relying on thermochemical conversion.

Given these challenges, greener solvents such as deep eutectic solvents (DES) have emerged as promising and environmentally compatible alternatives capable of selectively disrupting lignocellulosic matrices under mild conditions.[18] DES are liquids formed by combining hydrogen-bond acceptors (HBAs) and hydrogen-bond donors (HBDs), whose strong hydrogen-bond interactions induce a significant melting-point depression relative to the pure components.[19]

Beyond their effectiveness, DES are often characterized by low vapor pressure, reduced flammability, and, in many cases, low toxicity and good biodegradability, particularly when derived from inexpensive and readily available components. Their tunable polarity, acid−base balance, and solvation capacity enable the rational design of solvent systems with enhanced selectivity, offering advantages over conventional organic solvents in terms of safety, environmental impact, and process sustainability.[20] These features make DES especially attractive for selective biomass fractionation within integrated and sustainable biorefinery concepts.

Studies employing DES- or ionic liquid-based strategies for the processing of lignocellulosic residues,[21,22] including applications to sugar cane bagasse delignification,[23−25] have predominantly focused on conventional choline chloride (ChCl)-based DES, particularly ChCl:glycerol and ChCl:urea.[24] Acidic DES, including ChCl:oxalic acid and ChCl:trifluoroacetic acid,[26] as well as DES based on quaternary ammonium salts, such as triethylbenzyl ammonium chloride (TEBAC) combined with lactic acid,[27] have also been reported for sugar cane bagasse pretreatment, showing high delignification efficiencies under optimized conditions. In the TEBAC:lactic acid approach,[27] an initial liquid hot water step is combined with a subsequent DES stage, primarily aiming to maximize the release of fermentable sugars and ethanol production. In these approaches, process performance is typically assessed using metrics such as glucose and xylose concentrations, enzymatic conversion, ethanol yield, and mass balances directed toward biofuel generation. Such pretreatment strategies generally operate under relatively severe conditions, involving high temperatures, acidic DES treatment stages, and additional washing steps to remove the solvent and solubilized compounds prior to enzymatic saccharification. Therefore, the resulting cellulose- or holocellulose-rich solids are predominantly intended for downstream conversion.

Although lignin can be recovered and occasionally characterized following DES pretreatment, it is most often regarded as a secondary byproduct of processes primarily optimized for carbohydrate release. As a result, limited attention has been devoted to its structural integrity, purity, or functional potential. Despite the advances achieved with conventional DES pretreatment systems, strategies explicitly designed to enable the simultaneous and selective recovery of both holocellulose and functionally preserved lignin under mild operating conditions remain limited. In particular, the integration of thermodynamically guided solvent selection into dual-target fractionation frameworks has not been systematically addressed. Such a perspective broadens the criteria used to evaluate process performance, shifting the focus from exclusively sugar- and ethanol-centered metrics toward the integrated valorization of both biomass fractions.

However, implementing such a dual-target fractionation strategy critically depends on the rational selection of highly selective DES, a task complicated by the vast number of possible HBA:HBD combinations and the highly specific, nonideal interactions between their components. These constraints make purely empirical screening impractical and limit many reported studies. Accordingly, large-scale screening using the conductor-like screening model for real solvents (COSMO-RS), a quantum-chemistry-based predictive tool that estimates solvation properties directly from molecular structure, provides a rational strategy to narrow the DES chemical space prior to experimental validation, thereby moving beyond the trial-and-error approaches commonly employed in DES development for biomass fractionation.[28,29] Although COSMO-RS has previously been applied to solvent selection for lignin dissolution and related applications, its systematic integration into a selective fractionation framework targeting dual recovery has not been comprehensively evaluated.

In this context, this work aimed to address these limitations by developing a mild and selective DES-based delignification approach for sugar cane bagasse, guided by thermodynamic solvent screening to enable the simultaneous recovery of holocellulose and functionally preserved lignin. The COSMO-RS model was used to screen 47,080 DES combinations and identify those with the highest predicted affinity for lignin. The most promising DES was subsequently validated experimentally to assess its lignin removal efficiency and its ability to preserve the holocellulose-rich fraction. The operating conditions were further optimized using response surface methodology (RSM). The holocellulose-rich solids were characterized by Fourier transform infrared spectroscopy (FTIR), scanning electron microscopy (SEM), energy-dispersive X-ray spectroscopy (EDS), and thermogravimetric analysis (TGA). The recovered lignin was also characterized andevaluated as a biosorbent for the removal of the herbicide 2,4-dichlorophenoxyacetic acid (2,4-D). This integrated computational−experimental framework demonstrates the potential of selective DES fractionation within sustainable biorefinery concepts.

2. MATERIALS AND METHODS

2.1. Materials

Sugar cane (*Saccharum officinarum* L., variety CTC9002) was obtained from the Sugarcane Studies Center (NECANA) at the Federal University of Lavras, Minas Gerais, Brazil. The stalks were manually peeled with a knife to remove the outer fibrous layer (rind) and then ground in a roller mill for juice extraction. The resulting rind-free bagasse, hereafter referred to as SGB, was washed with distilled water and dried at 60 °C to constant mass. A fraction of bagasse containing the outer fibrous layer (rind-containing bagasse, SGB-C) was retained and prepared in the same manner for comparative purposes. Both dried biomasses were milled in a knife mill equipped with a 40-mesh sieve and stored in airtight containers. Compositional characterization of SGB and SGB-C was performed following the National Renewable Energy Laboratory (NREL) protocols for structural carbohydrates and lignin, with minor

https://doi.org/10.1021/acssuschemeng.6c00062
ACS Sustainable Chem. Eng. XXXX, XXX, XXX−XXX

adaptations, and TAPPI standards for holocellulose determination. Detailed procedures and compositional data are provided in Section S1.1 of the Supporting Information. All reagents were of analytical grade (>95% purity) and are listed in Table S1.

2.2. COSMO-RS Simulations

The COSMO-RS thermodynamic model, grounded in quantum chemistry, was applied to screen solvents with potential to promote sugar cane bagasse delignification, using predictive solvation metrics as the selection criterion. Geometry optimizations and charge density calculations for all species were performed in Turbomole (TmoleX19, v4.5) at the COSMO-BP-TZVP level, generating the surfaces required for subsequent analyses. Lignin used in the simulations was defined based on its monomeric units (H, G, and S), as reported in the literature,[30] adopting Guaiacylglycerol-β-guaiacyl ether (GG), corresponding to the β-O-4 motif, as the model compound to reflect the predominant aryl ether connectivity in lignin.[29,31] Simulations were carried out in COSMOtherm (version 21.0) with the BP_TZVP_21 parametrization.

A database comprising 214 HBAs and 220 HBDs was assembled, from which 47,080 potential DESs were generated by considering all possible binary combinations (1:1), to investigate their solvation effects on lignin model compound (GG). Solvent-lignin affinity was inferred from the infinite-dilution activity coefficient of the GG model, γ^{∞}. Combinations with lower $\ln(\gamma^{\infty})$ values were prioritized as indicative of greater solvation capacity and, therefore, greater potential to promote sugar cane bagasse delignification. COSMO-RS was applied at 25 °C for relative ranking of DES candidates, and experimental validation under delignification conditions (~100 °C) ensured the reliability of solvent selection.

2.3. Solvent Selection and Delignification Tests

Based on COSMO-RS predictions, 35 DES candidates were selected from combinations of five HBAs and seven HBDs (Table S1). In addition, HBA:HBD combinations that have not been previously reported or remain scarcely explored in the literature were preferentially selected, with the aim of developing novel DES formulations for biomass fractionation. Each DES candidate, prepared as an HBA:HBD mixture at a 1:1 molar ratio, was heated at 60−100 °C for 1−3 h under continuous stirring (Table S2). Mixtures that remained liquid and homogeneous after cooling were evaluated for water miscibility, and those that formed fully transparent solutions after water addition were selected for subsequent steps.

This screening resulted in 11 DESs (highlighted in bold in Table S2) selected for the preliminary delignification tests. For comparison, urea:propionic acid (U:PA, 1:2)[32] and choline chloride:lactic acid (ChCl:LA, 1:5),[23] which have been reported as effective alternative solvents for delignification, were included and prepared according to the literature. For the initial delignification tests, all DESs were acidified with p-toluenesulfonic acid (PTSA, 0.005 mol L^{-1}) following a procedure adapted from Soares et al.[32] A 3% w v^{-1} NaOH solution was evaluated as the benchmark.[33]

Delignification assays were carried out using SGB in a Radleys Tech Carousel at a solid-to-liquid ratio of 1:10, 90 °C and 90 min,[33] under constant stirring (600 rpm). After delignification, the solid fraction was washed twice with a hydroethanolic solution (40:60, v v^{-1}), centrifuged at 4 °C and dried at 105 °C to constant mass. All delignification experiments were performed at least in duplicate to allow calculation of mean values and standard deviations.

2.4. Optimization of Delignification Operating Conditions

The DGDE:ET + PTSA DES, selected based on the results of the initial solvent screening (see Section 3.3.1 for discussion), was subjected to response surface methodology (RSM) to systematically evaluate the influence of operational variables on lignin solubilization. A central composite rotatable design (CCRD) of the 2^3 type was adopted. The independent variables were DGDE molar fraction (X_1, 0−1), extraction temperature (X_2, 70−100 °C) and PTSA concentration (X_3, 0−0.10 mol L^{-1}). The design consisted of 17 experiments comprising factorial, axial and central points. The actual and coded levels of each variable are provided in Tables S3 and S4. All other operational parameters were kept constant to those used in the initial screening described in Section 2.3 (extraction time of 90 min and a solid-to-liquid ratio of 1:10).

Optimization considered two responses, holocellulose content, H (Y_1) and the integrated FTIR band area at 834 cm^{-1}, A_{834} (Y_2), representing polysaccharide preservation and lignin removal. Additional variables, including solubilized biomass mass, m_{sol}, and the solid fraction coloration, were monitored during the delignification. All of them are described in Section 2.5. The selected responses were fitted to the second-order polynomial model shown in eq 1:

$$y = \beta_0 + \Sigma_{i=1}^{k}\beta_i X_i + \Sigma_{i=1}^{k}\beta_{ii} X_i^2 + \Sigma_{i<i}^{k}\beta_{ij} X_i X_j \quad (1)$$

where β_0 is the intercept, β_i are the linear coefficients, β_{ii} are the quadratic coefficients, and β_{ij} are the interaction coefficients, and X_i and X_j are the independent variables.

The experimental data were analyzed at a confidence level of 95%. Model fitting and statistical evaluation were performed using ANOVA based on the coefficient of determination (R^2), F-value and p-value. Response surface and contour plots were generated to visualize the effects of the variables and to support the identification of operating regions associated with higher delignification selectivity. All statistical analyses and graphical outputs were carried out using Statistica software, version 12 (StatSoft Inc., Tulsa, USA). The operating conditions predicted by the model were validated experimentally.

The optimization was carried out using SGB, and the optimized conditions were subsequently applied to SGB-C to assess robustness. Under the same conditions, additional delignification assays were performed using ET + PTSA and a 3% w v^{-1} NaOH solution to allow direct comparison with the optimized DES + PTSA.

After determining the optimal operating point, kinetic experiments (30−360 min) were performed under the optimized conditions using H and A_{834} to monitor delignification progress.

2.5. Procedures for Delignification Evaluation

Gravimetric analysis was used to quantify the solubilized mass (m_{sol}) according to eq 2:

$$m_{sol} = m_i \times \left(1 - \frac{U}{100}\right) - m_{sf} \quad (2)$$

where m_i is the initial wet mass of the sample (g), U is the moisture content (%) and m_{sf} the mass of the resulting solid fraction (g).

FTIR (PerkinElmer, USA) was used to monitor changes in lignin-associated bands in the treated solids. Spectra were collected between 400 and 4000 cm^{-1} (2 cm^{-1} resolution, 32 scans). The area of the band at 834 cm^{-1} (A_{834}), attributed to out-of-plane C−H bending in para-substituted benzene rings, such as para-substituted guaiacyl and syringyl units, was selected as a specific marker for delignification. The band at 1511 cm^{-1}, commonly assigned to aromatic C=C stretching vibrations of lignin, was not used due to overlap with cellulose and hemicellulose bands. The value of A_{834} was obtained by integrating the 845−825 cm^{-1} region. Before integration, spectra were normalized (0−1 scale), baseline-corrected and smoothed using the Savitzky-Golay method (second-order polynomial, 15-point window). All spectral processing and integration were performed using Origin 2024b software. Lower integrated area values were interpreted as indicative of higher delignification.

In addition, the solid fractions obtained after delignification with the best-performing solvents identified from the gravimetric and FTIR analyses, as well as those obtained with the benchmark (NaOH solution), were also analyzed for holocellulose content (H (wt %)), which was determined according to eq 3:

$$H = \frac{m_{holo}}{m_{sf}} \times 100 \quad (3)$$

where m_{holo} is the dry mass (g) of the holocellulosic fraction obtained after sodium chlorite/acetic acid treatment, and m_{sf} is the mass (g) of the solid fraction. Details of the procedure are provided in Section S1.1.

https://doi.org/10.1021/acssuschemeng.6c00062
ACS Sustainable Chem. Eng. XXXX, XXX, XXX−XXX

The solid fraction coloration on a 0−1 scale (where 0 corresponds to dark brown and 1 corresponds to white) was also used as a qualitative indicator of holocellulosic preservation.

2.6. Lignin Recovery by Precipitation

The extracts from SGB and SGB-C obtained under the optimized conditions using the DGDE:ET + PTSA were subjected to the precipitation procedure for lignin recovery. For comparison, extracts obtained under the same optimized conditions using ET + PTSA and 3% w v^{-1} NaOH solution were processed in the same way.

Initially, each extract was diluted with ∼60 mL water, while the corresponding solid fraction was washed with the hydroethanolic solution described in Section 2.3. The aqueous extract, containing the solvent together with the solubilized lignin and other residues, was cooled in an ice bath, followed by the gradual addition of 2 mol L^{-1} H_2SO_4 until turbidity appeared (pH ∼ 10). The suspension was left to stand for approximately 1 h and was then concentrated in an oven at 60 °C for ∼10 h to promote partial evaporation of water. This procedure resulted in a pasty mixture, which was redispersed in distilled water at room temperature (∼25 °C). The suspension was centrifuged at 4000 rpm for 20 min, and the precipitated lignin was washed with distilled water until neutral pH, dried in an oven, and ground with a mortar and pestle. The supernatant was collected and concentrated again in an oven. This sequence of oven concentration, redispersion in water, centrifugation and washing was repeated three times to ensure maximum recovery of lignin.

2.7. Characterization of Solid Fractions

Holocellulosic and lignin solid fractions obtained under the optimized conditions with DGDE:ET + PTSA, ET + PTSA and 3% w v^{-1} NaOH for both SGB and SGB-C, together with them *in natura* counterparts, were characterized by Fourier-transform infrared spectroscopy (FTIR), scanning electron microscopy (SEM), energy-dispersive X-ray spectroscopy (EDS), and thermogravimetric analysis (TGA). CHNS elemental analysis and nuclear magnetic resonance (NMR) spectroscopy were performed exclusively on the lignin fractions, while color analysis was applied only to the holocellulosic fractions. Detailed descriptions of these procedures are provided in the Supporting Information (Section S1.2).

2.8. Herbicide Adsorption Assays

Adsorption assays were performed using different solid materials obtained as biosorbents, including original SGB, precipitated lignin obtained from SGB delignification under optimized conditions using DGDE:ET + PTSA, ET + PTSA and 3% w v^{-1} NaOH solution, as well as the corresponding holocellulosic fractions resulting from each treatment. In addition, two sugar cane bagasse biochars produced at 400 and 600 °C (BC400 and BC600), in accordance with previous studies,[9,34] were evaluated. Adsorption experiments were carried out by dispersing a known mass of adsorbent in 10.00 mL of an aqueous solution of 2,4-D (10.0 mg L^{-1}) at a solid-to-liquid ratio of 2.0 g L^{-1}.

All experiments were performed in glass bottles under constant agitation (120 rpm) in a shaker incubator (model NT715, Nova Técnica, Brazil). The adsorption conditions were maintained at pH 6.0, with a contact time of 24 h and a temperature of 25 °C. After the adsorption period, the suspensions were centrifuged at 4000 rpm for 5 min (Kasvi, model k14-0815P, Brazil), and the supernatants were collected for analysis. The residual concentration of 2,4-D was determined by UV−vis spectrophotometry (Shimadzu, model UV-1900i, Japan) using a 1 cm quartz cuvette at the maximum absorption wavelength of 284 nm. The equilibrium adsorption capacity, q_e (mg g^{-1}), and the percentage removal, R (%), of the herbicide were calculated according to eqs 4 and 5, respectively:

$$q_e = \frac{(C_i - C_e) \times V}{m} \tag{4}$$

$$R = \left(\frac{C_i - C_e}{C_i}\right) \times 100 \tag{5}$$

where C_i and C_e are the initial and equilibrium concentrations (mg L^{-1}), respectively, m is the mass of the adsorbent (g), and V is the solution volume (L).

3. RESULTS AND DISCUSSION

3.1. Compositional Analysis and Characterization of Sugar Cane Bagasse

To quantitatively assess the delignification behavior of the two biomasses, the compositional and structural properties of SGB and SGB-C were first determined. The compositional analysis (Table S5) reveals pronounced differences between the materials, with direct implications for cell wall architecture, solvent accessibility, and biomass recalcitrance. SGB contains nearly twice the proportion of water-soluble extractives (44.0% vs 23.2%), which may contribute to a less consolidated lignocellulosic matrix. Extractives can act as natural plasticizing agents and their partial removal is known to increase porosity and reduce intermolecular cohesion within the lignin-carbohydrate complex network, thereby facilitating solvent diffusion and enhancing lignin accessibility during pretreatment.[35]

In contrast, SGB-C exhibits substantially higher holocellulose (49.0% vs 34.0%) and Klason lignin contents (21.8% vs. 14.5%), consistent with a higher degree of lignification, secondary cell wall thickening, and structural density characteristic of rind tissues.[36] The elevated lignin content is particularly relevant, as lignin forms a hydrophobic, cross-linked matrix that restricts solvent penetration and shields carbohydrate polymers. Moreover, stronger lignin−hemicellulose associations in more lignified tissues can further increase structural rigidity and resistance to fractionation.[37] These features contribute to the greater recalcitrance of SGB-C and may limit delignification efficiency under equivalent operating conditions. The Klason lignin determined by compositional analysis was considered as the total lignin content in the biomass sample, and the lignin recovered and discussed in Section 3.5.1 is expressed relative to this total amount.

Conversely, the lower lignin content and higher extractives fraction in SGB suggest a structurally less recalcitrant material, which is expected to favor selective lignin removal under milder condition.[38] The small differences in moisture content (2.60% for SGB and 1.70% for SGB-C) are unlikely to significantly affect reactivity, while the similar ash contents in both biomasses (∼1%) indicate that inorganic constituents do not play a dominant role in the observed differences, particularly considering the low mineral fraction relative to the organic matrix.

FTIR spectra of both biomasses (Figure S1) exhibited characteristic lignocellulosic bands (Table S6), including O−H stretching (∼3300 cm^{-1}), aliphatic C−H stretching (∼2920 cm^{-1}), hemicellulose C═O stretching (∼1730 cm^{-1}), lignin aromatic vibrations (1600−1510 cm^{-1}), C−H deformations and C−O stretching of carbohydrates (1450−1320 cm^{-1}), as well as polysaccharide backbone signals (1200−900 cm^{-1}) and aromatic C−H out-of-plane bands (∼870−830 cm^{-1}).[39−45] SGB-C showed more pronounced aromatic and carbonyl bands and stronger signals below 600 cm^{-1} associated with silica and mineral components. These features are consistent with its higher lignin and inorganic contents and with the greater structural complexity of the rind-rich outer layer, which contains waxes, phenolics and mineral fractions known to hinder solvent diffusion.

https://doi.org/10.1021/acssuschemeng.6c00062
ACS Sustainable Chem. Eng. XXXX, XXX, XXX−XXX

Thermogravimetric analysis (Figure S2) further highlighted these distinctions. Although both biomasses displayed the typical three-stage degradation profile,[46] SGB released moisture at a lower temperature (87 °C vs 115 °C). In the hemicellulose/cellulose decomposition range (200−450 °C), SGB degraded more slowly and over a broader temperature range, whereas SGB-C degraded faster, reflecting its higher holocellulose content and greater thermal reactivity.[46,47] At higher temperatures, SGB-C (i.e., richer in lignin) showed greater late-stage mass loss (564−700 °C), while SGB retained more char residue (17% vs 10%), suggesting that extractives in SGB promote secondary charring, whereas the rind-rich SGB-C matrix favors volatilization.[48,49]

SEM micrographs (Figure S3) revealed heterogeneous, fibrillar morphologies typical of sugar cane bagasse,[50] without major structural differences attributable to rind content. EDS analysis confirmed oxygen-rich surfaces for both biomasses, while SGB-C contained small amounts of magnesium and calcium consistent with rind-derived mineral components.[51]

3.2. COSMO-RS Screening Results

COSMO-RS was employed as a thermodynamic screening tool to minimize trial-and-error experimentation by prioritizing HBA:HBD combinations based on the predicted activity coefficient at infinite dilution (γ^{∞}) of the lignin model in different solvents. The GG lignin model, widely used to simulate lignin−solvent interactions,[29] was applied to estimate solvation tendencies and identify the most promising candidates. Lower γ^{∞} values indicate stronger lignin−solvent interactions and a more favorable Gibbs free energy change of solvation.

The screening revealed that the identity of the HBA exerted a much stronger influence on predicted lignin affinity than the choice of HBD. This trend is clearly visible in the heat map (Figure S4), where horizontal banding indicates that varying the HBA causes much larger shifts in predicted affinity than varying the HBD. Among the HBAs evaluated, halogenated ammonium and phosphonium salts, followed by choline-based salts, exhibited the highest predicted affinity, consistent with their expected interactions with lignin aromatic domains (i.e., phenolic units).[52,53] Therefore, the HBAs considered and prepared to assess eutectic formation included 2-phenoxyethanol, tetrabutylphosphonium chloride, L-lysine, potassium carbonate and polyether-based acceptors such as diethylene glycol dimethyl ether, triethylene glycol dimethyl ether and tetraethylene glycol dimethyl ether.

The influence of the HBD was more modest. Urea and its derivatives showed the strongest predicted affinity, likely due to their ability to form multiple hydrogen bonds with lignin hydroxyl and carbonyl groups. Other HBD families, including amides, amino acids and peptides, sugars and polyols, nitrogen-containing heterocycles, and vitamin-derived compounds, also presented relevant solvation tendencies in the COSMO-RS screening.[54] Based on these trends, the HBDs considered and prepared to assess eutectic formation comprised 1,3-butanediol, butyric acid, tetramethylurea, ethanolamine, triethanolamine, dimethylformamide, fenchone, propionic acid and lactic acid.

The complete set of HBA:HBD combinations evaluated for the formation of stable eutectic mixtures is provided in Table S2, and their preparation check as detailed in Section 2.3.

3.3. Selective Delignification of Sugar Cane Bagasse

3.3.1. Initial Screening Using Selected Solvents. In the initial delignification screening of SGB, 11 DES acidified with PTSA (highlighted in bold in Table S2), previously validated for eutectic formation and water miscibility (Section 2.3), were evaluated. The incorporation of PTSA aimed to reduce thermal severity and improve experimental reproducibility. Preliminary experiments performed at 120 °C in the absence of PTSA led to pronounced darkening and partial degradation of the solid residue, impairing reproducible and quantitative fractionation and compromising the quality of the recovered holocellulosic fraction.

The chosen solvents covered a broad chemical space, including quaternary ammonium and phosphonium salts, diols and triols, amino acids, amides, amines, carboxylic acids, polyether-based acceptors, cyclic ethers, esters and organic carbonates. The literature DES U:PA and ChCl:LA[23,32] were included as references, and a 3% w v^{-1} NaOH solution[33] was used as the benchmark. Mild acidification with PTSA was applied to all DES to enhance lignin solubilization by promoting cleavage of lignin-carbohydrate linkages, thereby amplifying differences in selectivity among candidates, as commonly reported for acidic DES pretreatments.[23,32,55] The specific contribution of PTSA is analyzed in the following section.

Most DES promoted solubilization above the theoretical lignin mass, indicating coextraction of residual sugars and other minor constituents (Figure 1a). TBP:DMF + PTSA was the only DES that solubilized less than this theoretical value. In contrast, NaOH solubilized an amount very close to the theoretical lignin mass, reflecting its higher selectivity under the screening conditions. FTIR spectra of the solid fractions (Figure S5) showed characteristic changes in lignin-associated bands for all delignification media, confirming that the solubilization values correspond to effective delignification. Among the evaluated DES, DGDE:ET + PTSA produced the strongest decrease in the integrated FTIR band, A_{834}, indicating greater selectivity toward lignin removal. TBP:DMF + PTSA, despite its modest solubilization, exhibited non-selective removal of aromatic structures and was therefore excluded from further evaluation (Figure S5).

A direct comparison of the FTIR spectra obtained after treatment with DGDE:ET + PTSA and with 3% w v^{-1} NaOH (Figure 1b) revealed substantial attenuation or disappearance of lignin-associated bands at 1600, 1511, 863, and 834 cm^{-1} (Table S6), confirming the high delignification capacity of DGDE:ET + PTSA. Under the same screening conditions, the DES U:PA + PTSA[32] and ChCl:LA + PTSA,[23] previously reported in literature to be successful for the delignification of other types of wood biomass, did not achieve significant lignin removal for SGB.

To complement the FTIR analysis, the solid fractions obtained after delignification with DGDE:ET + PTSA and with 3% w v^{-1} NaOH were analyzed by determining their holocellulose content, H (wt %). These fractions, produced after the sodium chloride/acetic acid treatment, are hereafter denoted as H-X, where X corresponds to the delignification solvent. As expected for carbohydrate-enriched materials, the holocellulose content increased to approximately 83% for both H-DGDE:ET + PTSA and H-NaOH, compared with 37% for SGB (Figure 1c). These results support the FTIR observations, and the integrated FTIR band A_{834} proved to be an effective rapid-screening metric, enabling consistent comparison among

https://doi.org/10.1021/acssuschemeng.6c00062
ACS Sustainable Chem. Eng. XXXX, XXX, XXX−XXX

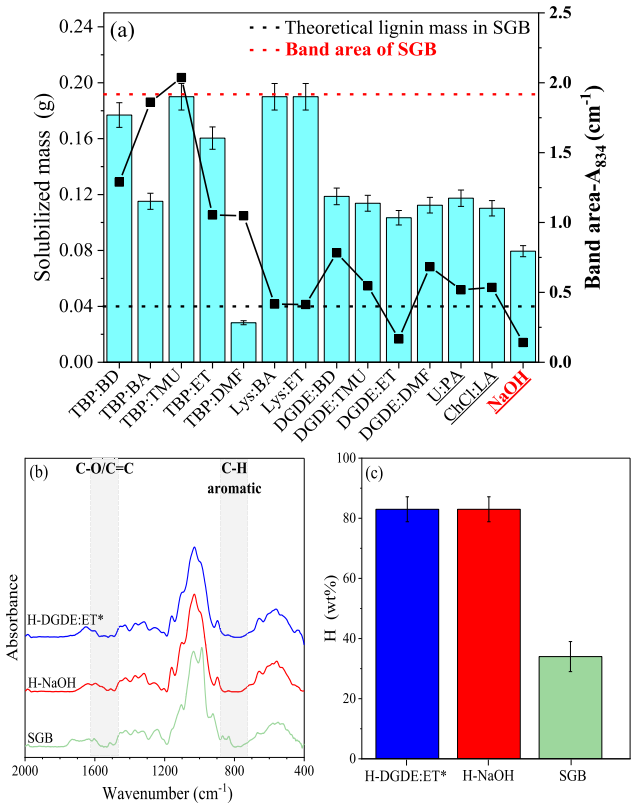

Figure 1. (a) Solubilized mass, m_{sol} (bars) and A_{834} from FTIR (dots) after treatment with different solvents (HBA:HBD + PTSA). Dotted lines indicate the same parameters for original SGB. (b) Representative FTIR spectra (magnification 2000−400 cm^{-1}) and (c) holocellulose content, *H*, in the solid fractions obtained after treatment with different solvents (H-X, X = solvent) and SGB *in natura*. Delignification conditions: 90 °C, PTSA 0.005 mol L^{-1}, HBA:HBD 1:1, 90 min, S/L ratio 1:10. NaOH was used at a concentration of 3% w v^{-1}. *Addition of PTSA.

solvents and clearly highlighting DGDE:ET + PTSA as the most selective medium. Furthermore, comparison of the FTIR spectra of DGDE:ET + PTSA and NaOH (Figure 1b; Table S6) indicates that the DES also removes soluble sugars without requiring additional washing steps, thereby reducing downstream operations and simplifying the overall process. Even before optimization, its delignification performance approaches that of NaOH solution, while operating under milder conditions and avoiding the production of strongly alkaline effluents.

Taken together, the screening results identify DGDE:ET + PTSA as the most promising solvent for the selective delignification of SGB. To understand the origin of this superior performance, the contributions of the DES components (HBA and HBD) and PTSA must be examined in greater detail.

3.3.2. Effect of Solvent Properties on Lignin Solubilization Process. To determine how the DES components contribute to the performance of DGDE:ET, the structural roles of the HBA and the HBD were examined. DGDE, a polar aprotic polyether that acts as a hydrogen-bond acceptor,[56] was replaced with TGDE and TeGDE, whereas ET, an amino alcohol capable of strong hydrogen-bond donation,[57] was replaced with TET. These variations were selected to probe the synergistic interactions between DGDE, ET and PTSA suggested by the screening step and to assess how HBA and HBD structure influence delignification efficiency and selectivity. Each DES was evaluated with and without PTSA to distinguish the influence of solvent structure from that of acid catalysis.

Increasing the HBD chain length from ET to TET resulted in higher solubilized mass (Figure S6), but this increase was not accompanied by improved selectivity. FTIR spectra (Figures S7 and S8) and holocellulose content (Figure S9) clearly show that the additional solubilization observed for TET-based DES arises from coextraction of nonlignin components rather than from more effective delignification. In contrast, DES formulated with ET, particularly DGDE:ET + PTSA, promoted a pronounced reduction in lignin-associated FTIR bands while preserving a higher proportion of the polysaccharide fraction. These differences reflect the distinct properties of the two HBDs: ET, which exhibits lower steric hindrance and higher basicity, favors the selective cleavage of lignin linkages, whereas TET promotes broader matrix dissolution that reduces selectivity.[58]

Importantly, the modest changes in solubilized mass upon PTSA addition indicate that acidification does not enhance bulk dissolution (Figure S6). The influence of PTSA becomes evident in the FTIR spectra and in the integrated band A_{834} (Figures S7 and S8), where PTSA consistently decreases lignin-associated bands. This confirms that the primary role of PTSA is to improve lignin selectivity rather than to drive extensive solubilization. Although PTSA enhanced delignification for both HBDs, high selectivity was observed only for ET-based DES, demonstrating that acid catalysis alone is insufficient to achieve selective lignin removal without an appropriate HBD.

Overall, the results show that DGDE:ET + PTSA provides the most favorable balance between lignin solubilization and preservation of the polysaccharide fraction among the DES evaluated. Because DGDE:ET + PTSA was identified as the most effective delignification medium, its structural integrity and thermal stability were assessed before proceeding with process optimization. The FTIR spectrum of DGDE:ET + PTSA (Figure S10) corroborates the formation of the eutectic mixture, displaying characteristic bands of sulfonated groups (S═O at 1355−1300 and 1248−1199 cm^{-1}, S−O bending at 537−430 cm^{-1}),[55] as well as bands associated with the aromatic ring of PTSA (C═C at 1597 cm^{-1} and out-of-plane C−H at 853 cm^{-1}). Additional contributions from ether and alcohol groups (C−O−C/C−O at 1103−1029 cm^{-1} and 935−964 cm^{-1}), aliphatic CH_2/CH_3 deformations and stretching vibrations (1455 cm^{-1} and 2919−2827 cm^{-1}, respectively), and a broad O−H/N-H band at 3355−3293 cm^{-1} were also observed, supporting the presence of strong hydrogen-bonding interactions between the DES components.[59]

The thermal stability of DGDE:ET + PTSA was assessed by TGA (Figure S11), which showed an initial water-loss event near 103 °C, followed by decomposition around 141 °C and further mass loss near 170 °C. The final residue at 700 °C was 4.2%. These results indicate that DGDE:ET + PTSA performs best under mild temperature conditions (≤100 °C), which aligns with the delignification conditions employed in this work. Together, these findings confirm DGDE:ET + PTSA as a stable and sustainable solvent for the subsequent optimization of SGB delignification.

3.3.3. Optimization of the Operational Conditions. RSM was applied to optimize the delignification of SGB using

https://doi.org/10.1021/acssuschemeng.6c00062
ACS Sustainable Chem. Eng. XXXX, XXX, XXX−XXX

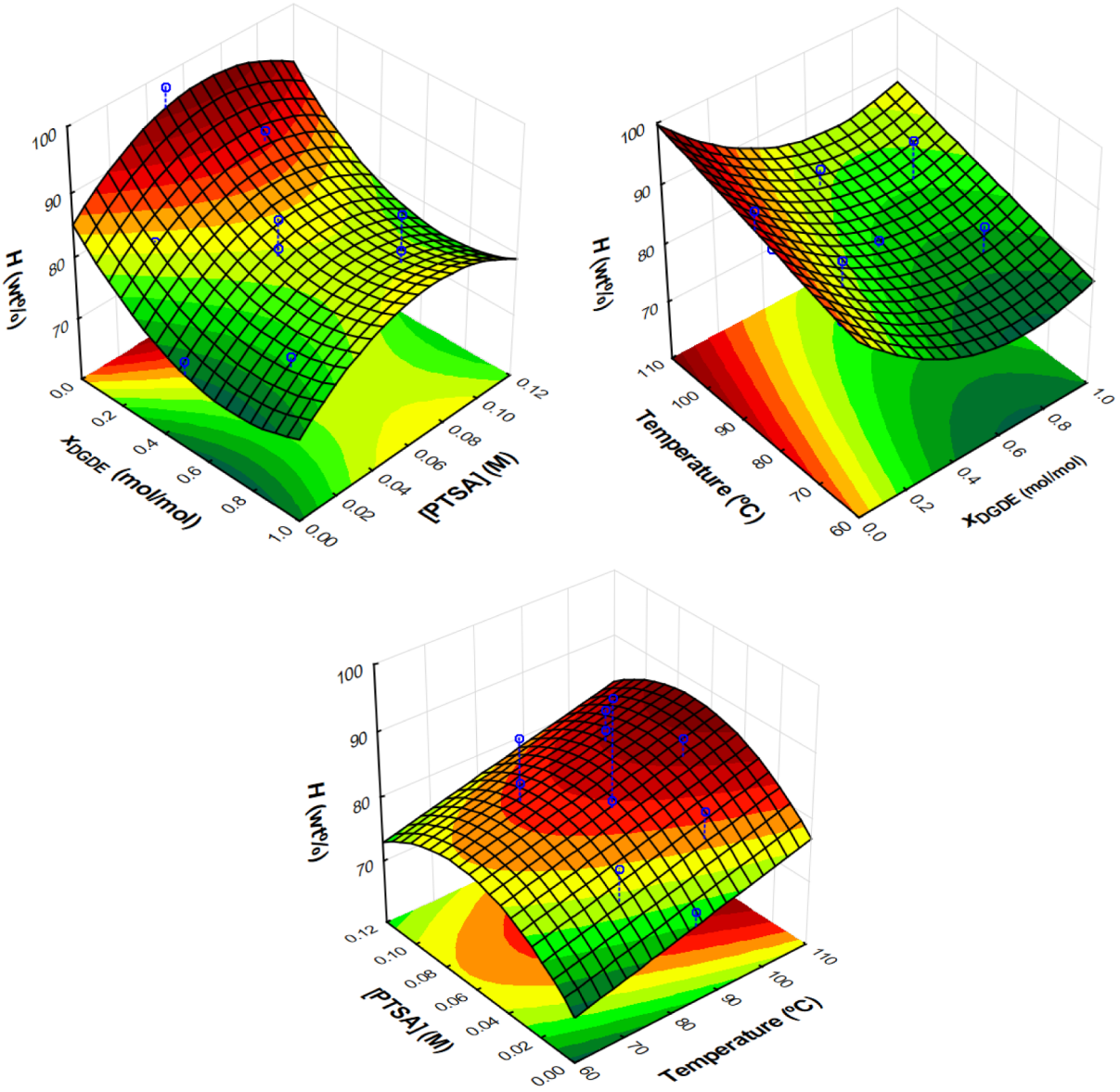

Figure 2. Response surfaces and contour maps for *H*. 3D surfaces of holocellulose as a function of DGDE molar fraction (X_1) × temperature (X_2) at the central level of PTSA concentration (X_3); X_1 × PTSA concentration (X_3) at central temperature (X_2); and $X_2 \times X_3$ at central of DGDE molar fraction (X_1). Color scale denotes holocellulose level (green = lower; red = higher).

the most promising solvent, DGDE:ET acidified with PTSA. The effects of DGDE molar fraction (X_1), temperature (X_2) and PTSA concentration (X_3) were evaluated to identify the conditions that maximize selectivity. Selectivity was quantified using two response variables, holocellulose content, *H* (Y_1) and the integrated FTIR band area at 834 cm^{-1}, A_{834} (Y_2), which represent polysaccharide preservation and lignin removal, respectively. Additional responses, such as solubilized mass and solid fraction coloration, were monitored but not included as optimization criteria. Solubilized mass may include contributions from coextracted nonlignin components (Section 3.3.2), and coloration is qualitative and therefore less reliable. Experimental data for all RSM runs are provided in Table S7, and the corresponding polynomial models are summarized in Table S8. Table S9 presents the corresponding additional responses.

The fitted models exhibited good representativeness, with R^2 values of 0.76 for *H* and 0.91 for A_{834} (Figures S12 and S13; Table S8). ANOVA (Tables S10 and S11) confirmed the statistical significance of both models and showed that temperature (X_2) was the dominant factor governing lignin removal. The negative coefficient for X_2 in the A_{834} model indicates that higher temperatures lead to a decrease in lignin-associated absorbance. In contrast, DGDE molar fraction (X_1) primarily influenced *H*, with higher values reducing holocellulose preservation. PTSA concentration (X_3) produced a modest positive effect on *H*, and the presence of a quadratic term indicates slight curvature in this response. In accordance with the model structure, PTSA concentration (X_3) did not significantly influence A_{834}, and no interaction terms were significant. Collectively, these results indicate that the factors act largely independently, with temperature controlling lignin solubilization and solvent composition and PTSA contributing to polysaccharide stability.

The response surfaces in Figures 2 and 3 supports these findings. Figure 2 shows a broad high-response plateau for H at

https://doi.org/10.1021/acssuschemeng.6c00062
ACS Sustainable Chem. Eng. XXXX, XXX, XXX−XXX

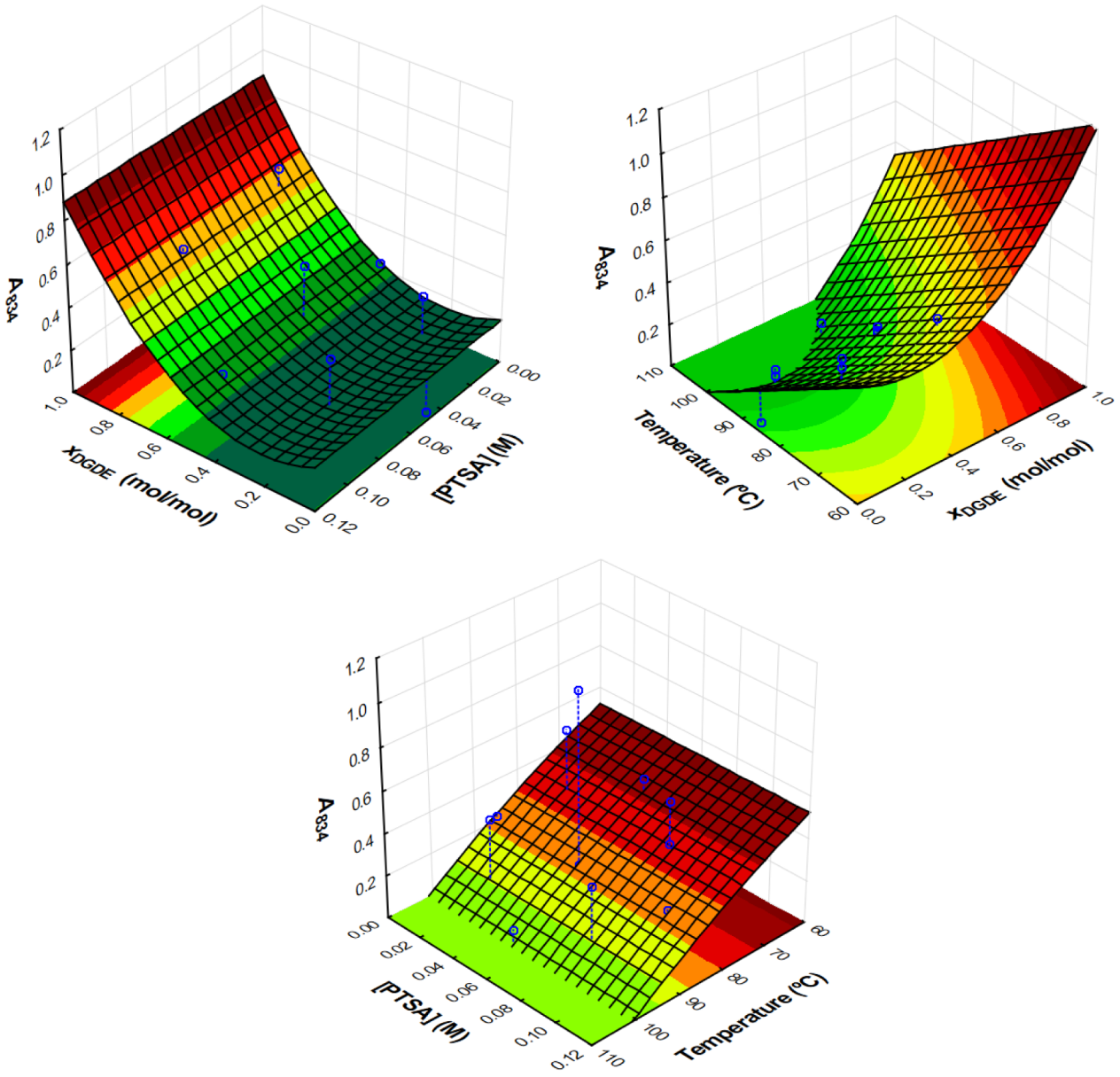

Figure 3. Response surface and contour map for the FTIR A_{834}. A_{834} as a function of DGDE molar fraction (X_1) and temperature (X_2), with [PTSA] (X_3) fixed at the central level. The color scale indicates A_{834} (green = lower; red = higher); lower values indicate reduced intensity of A_{834} and, by inference, greater delignification.

temperatures above 90 °C and DGDE molar fractions near 0.10, delineating conditions where holocellulose preservation remains consistently high. *H* decreased sharply at lower temperatures or at higher DGDE fractions, whereas the effect of PTSA remained secondary. Figure 3 presents the corresponding response surface for A_{834}, which displays a pronounced minimum at high temperatures and low DGDE molar fractions, conditions where ET predominates and lignin removal is maximized. Variations along the PTSA axis were minimal, consistent with the absence of X_3 in the A_{834} model. The visual appearance of the solids recovered after each RSM run (Figure S14) further supports these trends. Most samples exhibited similar coloration, except for run 9 (DGDE molar fraction = 0.0; 85 °C; PTSA concentration = 0.05 M), which appeared lighter. This observation is consistent with its exceptionally high holocellulose content (98%) and low A_{834}, indicating extensive lignin removal under ET-rich conditions.

Taken together, Figures 2 and 3 indicate a convergent operational region characterized by temperatures near 100 °C and DGDE molar fraction around 0.10, where holocellulose preservation is maximized and A_{834} minimized. These results suggest that lignin removal depends primarily on DGDE molar fraction (X_1) and temperature (X_2), while PTSA concentration (X_3) does not directly influence delignification, it instead fine-tunes holocellulose preservation.

The optimal operational conditions identified by RSM were a DGDE molar fraction of 0.1 (or molar ratio HBA:HBD of 1:9), a temperature of 100 °C and a PTSA concentration of 0.03 mol L^{-1}. Under these conditions, the experimental holocellulose content reached 88.9%, while the band at 834 cm^{-1} was completely suppressed, indicating extensive lignin removal. These experimental values closely matched the RSM predictions (91.2% for *H*; deviation 2.6%), confirming both the accuracy of the models and the effectiveness of DGDE:ET

https://doi.org/10.1021/acssuschemeng.6c00062
ACS Sustainable Chem. Eng. XXXX, XXX, XXX−XXX

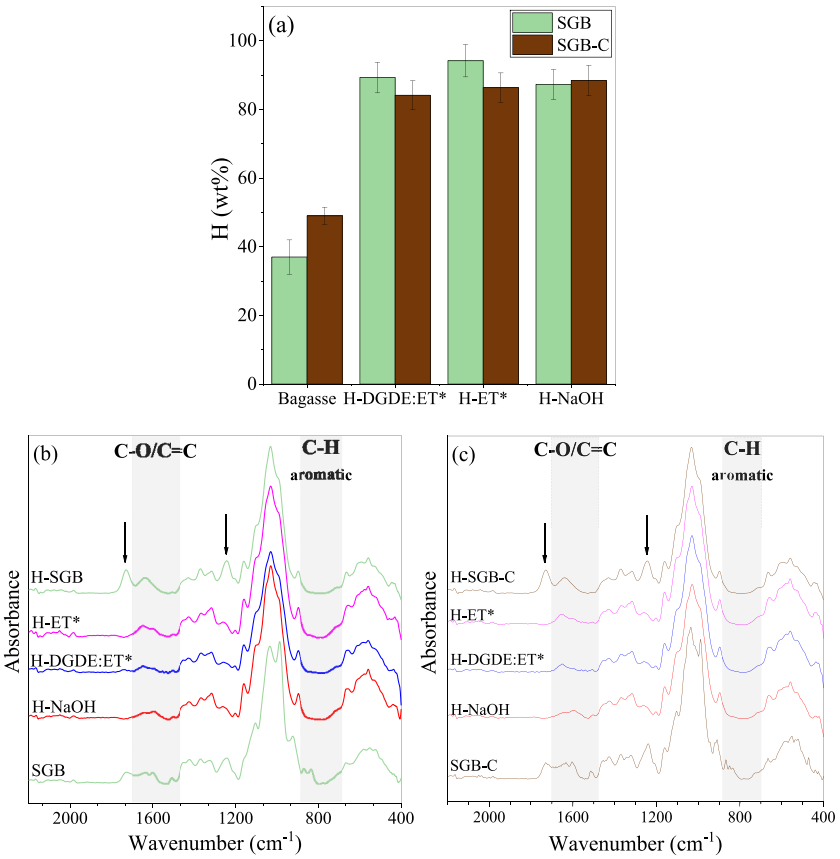

Figure 4. (a) *H* in the solid fractions obtained after treatment with different solvents in the SGB (or SGB-C); (b−c) Representative FTIR spectra (2200−400 cm^{-1}) of SGB (or SGB-C), solid fractions obtained after treatment with different solvents, and the holocellulose sample obtained by the conventional method from each bagasse (H-X, X = solvent used in the treatment or bagasse). Delignification in RSM-optimized conditions. *Addition of PTSA.

acidified with PTSA. Literature reports indicate that such efficient delignification at 100 °C is remarkably mild compared with other eutectic or ionic liquid media, which typically require 109−160 °C.[24,26,60]

Having established the optimal conditions, the next step was to examine the kinetic profile of the delignification process. As shown in Figure S15, lignin removal progressed rapidly during the first 30 min, with A_{834} decreasing by approximately 95%. Subsequently, A_{834} continued to decline until about 90 min, reaching values close to zero and remaining constant thereafter. The pronounced initial decrease, followed by stabilization near the detection limit, indicates that the process is heterogeneous and likely governed by rapid removal of surface-accessible lignin combined with diffusion-controlled mechanisms.[61] In contrast, H increased progressively, reaching a maximum at 90 min, and then declined slightly at longer extraction times, which can be attributed to hemicellulose hydrolysis and concomitant reductions in the cellulose degree of polymerization.[62,63]

Prolonged extraction times (270 and 360 min) caused marked changes in the morphology of the solid fraction (Figure S16), including darkening and increased stiffness, characteristic of humin or pseudolignin formation via sugar dehydration and polycondensation. These effects, combined with surface deposition and pore collapse following lignin depletion,[64,65] indicate that most extractable lignin had been removed by 90 min and that extended treatments primarily damage the holocellulosic matrix. Accordingly, an extraction time of approximately 90 min was selected as the optimal operating condition.

3.3.4. Comparison between Solvents and Biomass Types. Once the optimal conditions and extraction time had been established, the next step was to evaluate whether the solvent composition could be simplified without compromising performance. This analysis was motivated by the RSM results, which showed that delignification efficiency increased as the medium became richer in ethanolamine (lower DGDE molar fractions), as well as by the mechanistic insights (Section 3.3.2) indicating that ET is the major contributor to selective lignin removal. For this reason, DGDE:ET + PTSA was compared directly with ET + PTSA and with NaOH under the optimized conditions. Both SGB and SGB-C were included in the studies to assess whether the optimized medium remains effective under increased structural complexity. Figure 4a presents the comparison of the three solvents for both biomasses.

The comparison revealed clear differences in solvent behavior. ET + PTSA promoted extensive lignin removal but resulted in a slightly stiffer solid fraction. In contrast, DGDE:ET + PTSA provided a more controlled response, achieving extensive delignification while better preserving the structural integrity of the solid. These results indicate that ethanolamine is the primary delignifying agent in the medium, a behavior that is consistent with previous studies reporting the effectiveness of ET-based media, including ET-based DES,[57] ET-based ionic liquid and organic acid formulations applied to pineapple crown biomass,[66] and ET-based solvents used for

https://doi.org/10.1021/acssuschemeng.6c00062
ACS Sustainable Chem. Eng. XXXX, XXX, XXX−XXX

Table 1. Colorimetry of the Holocellulosic Fraction (L*, a*, b*) Under D65/10° in SGB and SGB-C

	D65 10° Lab					
	SGB			SGB-C		
Sample	L*	a*	b*	L*	a*	b*
H-bagasse[a]	82.48 ± 1.36	3.11 ± 0.56	15.53 ± 1.63	81.72 ± 0.92	2.65 ± 0.63	12.09 ± 0.21
H-DGDE:ET + PTSA	80.87 ± 1.95	1.11 ± 0.12	15.18 ± 1.03	72.00 ± 2.53	1.76 ± 0.23	16.24 ± 0.98
H-ET+PTSA	83.83 ± 0.97	-1.79 ± 0.16	16.57 ± 1.14	67.87 ± 1.21	4.89 ± 1.03	12.01 ± 2.56
H-NaOH	80.58 ± 1.01	-0.38 ± 0.09	15.88 ± 0.97	76.03 ± 0.78	0.10 ± 0.01	14.54 ± 1.34

[a]Holocellulose samples from SGB or SGB-C.

the selective delignification of *Camellia oleifera* shells.[67] Within DGDE:ET + PTSA, DGDE moderates the intrinsic reactivity of ethanolamine and enhances selectivity, in agreement with the trends identified through the RSM and the solvent–structure analysis discussed earlier. Compared with the alkaline benchmark, DGDE:ET + PTSA achieved similarly extensive lignin removal while operating under milder conditions and with reduced structural degradation.

With respect to biomass type, the A_{834} decreased to values close to zero for both SGB and SGB-C after treatment with DGDE:ET + PTSA, ET + PTSA and NaOH (Figure S17), confirming effective lignin removal regardless of rind content. Holocellulose contents also increased substantially relative to the original materials, reaching approximately 85–95% in SGB and 84–88% in SGB-C (Figure 4a). The slightly lower values obtained for SGB-C reflect its greater recalcitrance and the higher susceptibility of its hemicellulose fraction to losses during extended treatments.[68]

FTIR spectra of the solid fractions obtained from SGB and SGB-C (Figure 4b–c) further support these observations. Significant suppression of the hemicellulose-associated bands at 1730 and 1245 cm^{-1}[39,40] was observed in all fractions, while a weak residual band at 1511 cm^{-1}, characteristic of lignin, remained detectable. Combined with the compositional data for the original materials (Section 3.1), these spectral features indicate partial hemicellulose loss during processing and the persistence of small amounts of lignin in the treated solids (Section 3.4.1).

Despite the higher structural complexity of SGB-C, the optimized medium proved robust, as both biomasses reached high holocellulose contents and nearly complete suppression of A_{834}. If required, mild pretreatments such as wax removal or dilute-alkali washing could mitigate hemicellulose losses in rind-rich materials, although such steps are not essential to achieve efficient delignification with DGDE:ET + PTSA.

3.4. Holocellulosic Fraction

3.4.1. Characterization. Following delignification, the solid fraction was characterized to assess how each solvent influenced the composition and structure of the recovered material. These solid fractions are referred to as holocellulosic fractions (H-X, X = solvent) because they contain approximately 90% of holocellulose. Color analysis in the CIELab space (Table 1) was performed under illuminant D65 and a 10° observer according to CIE/ISO recommendations.[69] In this color space, L* quantifies lightness (0 = black, 100 = white), a* describes the green–red axis (negative values indicate greenness and positive values redness), and b* represents the blue–yellow axis (negative values indicating bluish and positive values yellowish tones). For SGB, ET + PTSA produced the brightest holocellulosic fraction and shifted a* toward green, while DGDE:ET + PTSA and NaOH yielded slightly darker materials. For SGB-C, all fractions were darker than the reference, and differences in L* and a* were more pronounced, reflecting the strong influence of rind on color development.

The FTIR spectra of the holocellulosic fractions (Figure 4b–c) exhibited strongly attenuated aromatic markers at 1510–1600 cm^{-1} and prominent carbohydrate bands at 1160–1025 cm^{-1}, with a well-defined β-glycosidic band at ∼898 cm^{-1}, characteristic of cellulose.[42] A decrease at ∼1730 cm^{-1}, corresponding to ν(C═O) of acetylated xylans, was observed in all samples, consistent with partial hemicellulose loss during treatment.[39,40] In SGB, ET + PTSA and DGDE:ET + PTSA reproduced the profile of the holocellulose reference, confirming effective lignin removal. In SGB, NaOH produced the greatest reductions in both aromatic and ∼1730 cm^{-1} signals, whereas DGDE:ET + PTSA and ET + PTSA showed intermediate behavior with residual aromatic bands, consistent with the higher recalcitrance of rind-containing biomass.

SGB-C displays more intense aromatic features and a more pronounced band at ∼1730 cm^{-1}. After treatment, NaOH produces the largest decreases in both 1510–1600 cm^{-1} and ∼1730 cm^{-1} band intensities, suggesting more efficient removal of lignin/extractives and concurrent extraction of hemicellulose in the presence of rind. DGDE:ET + PTSA and ET + PTSA show intermediate behavior, with residual aromatic signals at ∼1510 cm^{-1} (consistent with lignin remnants) and a relative gain of signal in the carbohydrate region.

SEM micrographs of SGB and SGB-C (Section 3.1) showed heterogeneous and partially agglutinated surfaces, composed of fragmented particles and fiber bundles established by the lignin sheath.[70] After delignification, clear morphological changes were observed in the holocellulosic fractions. For SGB (Figure 5), H-SGB (Figure 5a) displayed a more compact agglomerated structure, whereas all solvent-treated fractions (Figure 5b–d) consisted mainly of irregular and fragmented particles forming thin lamellar structures. This morphology indicates partial peeling of lignocellulosic fibrils and the creation of interlamellar voids, leading to increased surface roughness.[71] Among them, H-DGDE:ET + PTSA (Figure 5b) appeared less compact, with wider lamellar spacing similar to the H-SGB, while H-ET + PTSA (Figure 5c) and H-NaOH (Figure 5d) showed denser and more collapsed structures.

For SGB-C (Figure S18), the holocellulosic fractions retained a morphology closely resembling that of SGB-C, with compact fiber domains and fewer lamellar separations. This reflects the greater structural complexity imposed by the rind, which restricts fibrillar peeling and increases resistance to morphological changes during delignification.

EDS analysis (Tables S12 and S13) confirmed oxygen as the predominant element in all holocellulosic fractions. The

https://doi.org/10.1021/acssuschemeng.6c00062
ACS Sustainable Chem. Eng. XXXX, XXX, XXX–XXX

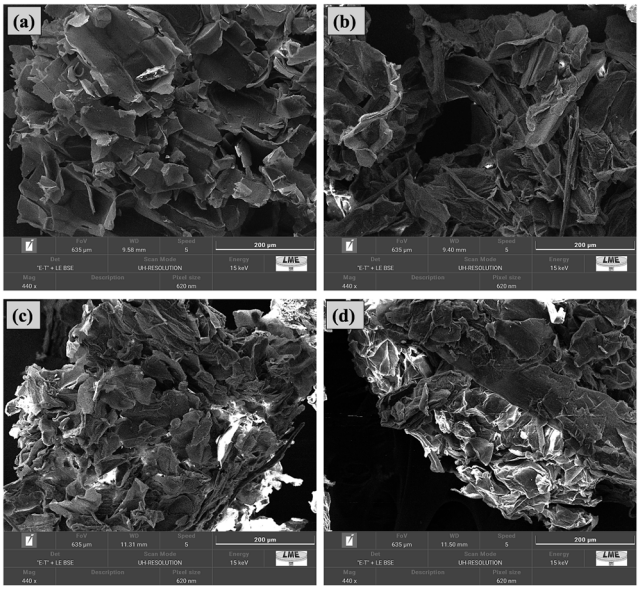

Figure 5. SEM images of holocellulosic fractions obtained from SGB: (a) H-SGB; (b) H-DGDE:ET + PTSA; (c) H-ET + PTSA; and (d) H-NaOH. H-X (X = solvent or bagasse) denotes the holocellulosic fractions obtained after delignification, including the holocellulose sample from the bagasse.

reference samples H-SGB and H-SGB-C contained traces of chlorine (≤5.29%), originating from the sodium chlorite/acetic acid bleaching process. In contrast, the H-DGDE:ET + PTSA, H-ET + PTSA and H-NaOH fractions contained only oxygen (carbon was subtracted), indicating efficient washing and removal of inorganic residues following delignification.

To further evaluate the thermal stability of the recovered materials, TGA analyses were performed on all holocellulosic fractions. H-SGB exhibited greater thermal complexity and a residual mass of 9%, indicating incomplete lignin removal (Figure S19a). In contrast, the fractions obtained with DGDE:ET + PTSA, ET + PTSA and NaOH, for SGB, displayed profiles characteristic of high-purity holocellulose, with cellulose-dominated degradation and residual masses of only 0−1% (Figure S19c−d). The H-DGDE:ET + PTSA fraction showed the lowest extent of degradation above 420 °C, suggesting more efficient removal of recalcitrant components. TGA analyses of the fractions obtained from SGB-C (Figure S20) revealed behavior comparable to that of rind-free biomass, indicating that the presence of rind did not significantly affect the thermal stability of the holocellulosic fractions.

Together, these results demonstrate that solvent selection not only governs compositional and morphological outcomes but also influences the thermal behavior and overall purity of the holocellulosic fractions.

It is important to highlight that the structural characterizations conducted here did not indicate significant alterations in the structure of the recovered holocellulose. This suggests potential susceptibility to enzymatic hydrolysis, which is widely applied in biofuel-oriented research. However, biomass drying may induce hornification and pore collapse, thereby reducing enzymatic accessibility and influencing hydrolysis outcomes.[72,73] Dedicated enzymatic assays are therefore required to accurately evaluate holocellulose digestibility. Enzymatic hydrolysis of the recovered holocellulose was not performed in this study and will be addressed in future work.

3.5. Lignin Fraction

3.5.1. Lignin Recovery by Precipitation. The precipitation of solubilized lignin from the selected solvent is essential both for full biomass utilization and for assessing solvent selectivity. However, this process has proven challenging. Different precipitation protocols have been reported, and Jardim et al.[74] showed that lignin precipitated at pH 2.5 exhibits higher purity than that obtained at pH 9.5. In the case of DGDE:ET + PTSA and ET + PTSA, which are highly basic media, strong buffering hindered pH adjustment and required large volumes of acid and water. At the same time, the low theoretical lignin concentration favored dispersion rather than aggregation, further impairing precip-

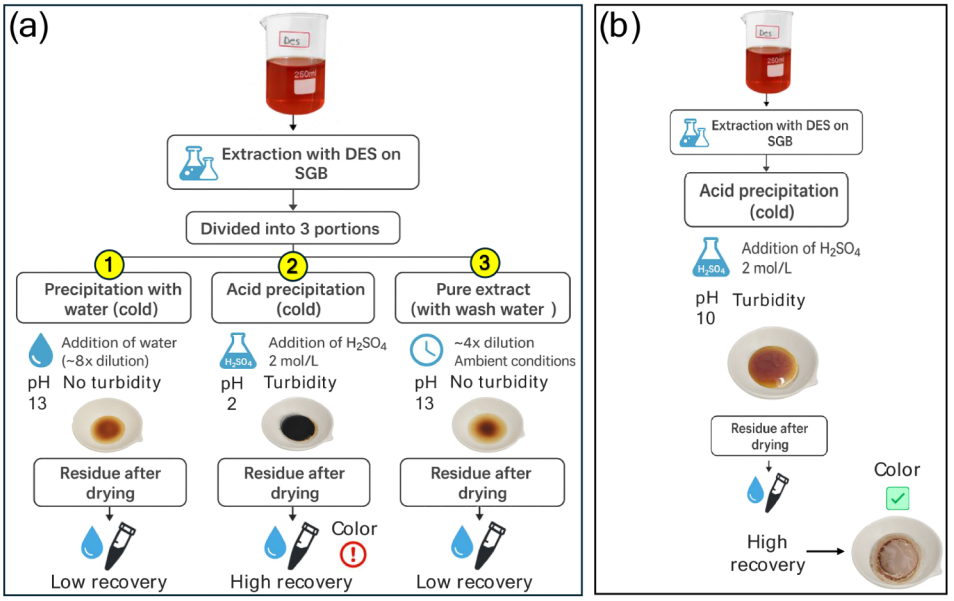

Figure 6. Workflows for lignin recovery from DES (DGDE:ET + PTSA) extracts of SGB; (a) fractionated approach and (b) proposed strategy. Lignin samples after each methodology are shown. Number inside the yellow circles indicates the evaluated routes.

https://doi.org/10.1021/acssuschemeng.6c00062
ACS Sustainable Chem. Eng. XXXX, XXX, XXX−XXX

itation efficiency. Under these conditions, cold-water addition alone did not generate a stable precipitate, since the solid tended to resolubilize in the basic medium. Direct solvent evaporation in a convection oven was also not feasible because DGDE:ET + PTSA has very low vapor pressure.[75,76]

Figure 6a summarizes the initial attempts to precipitate lignin from the DGDE:ET + PTSA extract obtained under optimal delignification conditions. Cold-water precipitation (route 1) and low-temperature acid precipitation (route 2)[77,78] were evaluated, but centrifugation (4000 rpm, 20 min) did not successfully isolate the dispersed solids. The unfractionated extract (route 3) similarly failed to dry completely, resulting in lignin remaining solubilized. Only at pH ≈ 2 (route 2) a water-insoluble material was formed, visually resembling Klason lignin, although reaching such a low pH required excessive dilution of the extract.

Given these limitations, an alternative approach was evaluated (Figure 6b). The extract was adjusted to pH 10, which produced visible turbidity, then dried at 60 °C for approximately 10 h and subsequently redispersed in water. This procedure enabled lignin precipitation while avoiding extensive acidification and excessive dilution. The resulting material exhibited a color similar to Kraft lignin, which may be beneficial for applications discussed in Section 3.6.

Lignin precipitation using this methodology was evaluated for extracts obtained from SGB and SGB-C treated with DGDE:ET + PTSA, ET + PTSA or 3% w v^{-1} NaOH. The lignin recovery yields are shown in Figure 7a. For SGB, ET + PTSA and DGDE:ET + PTSA showed overlapping confidence intervals (52.6−59.4% and 46.5−55.5%, respectively), indicating similar precipitation behavior. NaOH presented the lowest yield (40.95 ± 2.60%, confidence interval 38.3−43.5%), with no overlap relative to the DES-based media. For SGB-C, precipitation yields were generally lower. ET + PTSA and DGDE:ET + PTSA again showed overlapping confidence intervals (35.2−38.9% and 32.2−41.8%, respectively), whereas NaOH presented slightly higher yields (40.2−49.1%), with minimal overlap.

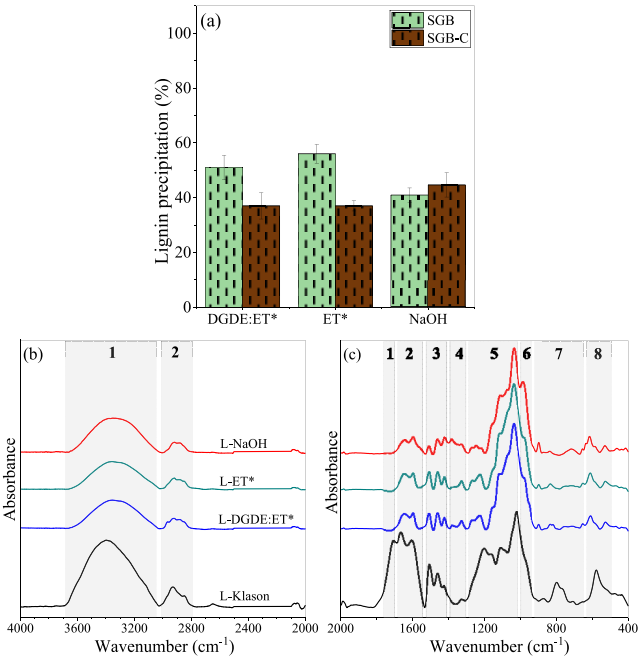

Figure 7. (a) Lignin precipitation yield expressed as percentage of the Klason lignin content determined by compositional analysis (100% basis); FTIR spectra of lignin from SGB: (b) Magnification 4000−2000 cm^{-1}, and (c) Magnification 2000−400 cm^{-1}. L-X denotes the lignin recovered using each solvent or obtained by the Klason method. The numbered areas in panels (b) and (c) indicate specific spectral regions discussed in the text. *Addition of PTSA.

Taken together, the results show that rind content reduces lignin recovery and impacts its precipitation efficiency. In SGB, precipitation was less hindered for the DES-based media than for NaOH, whereas in SGB-C the opposite was observed.

Most published studies do not explicitly consider the influence of rind, and lignin yields are typically reported for rind-containing bagasse. Nguyen-Thi,[33] for example, used 10% NaOH combined with thermal pretreatment. Here, without pretreatment and using only 3% NaOH, yields (~38%) were comparable to reported values following acid precipitation (H_2SO_4) and subsequent use of recovered lignin for dye and metal adsorption. In the context of DES, Sunar[26] reported lignin yields of 5.33 ± 1.30% and 39.51 ± 1.25% using choline chloride:oxalic acid and choline chloride:trifluoroacetic acid at 108−111 °C. These results, together with the present findings, suggest that the absence of rind favors higher yields, reinforcing the impact of biomass anatomy on the precipitation step.

Overall, DES-based delignification studies[21−25] have focused primarily on delignification efficiency and the performance of the holocellulosic fraction, whereas lignin precipitation has received comparatively little attention. The present results emphasize the importance of lignin recovery as an informative parameter for understanding solvent−biomass interactions.

3.5.2. Physicochemical Characterization. In addition to the holocellulosic fraction, the lignin recovered after delignification was also characterized to determine how each solvent and precipitation condition influenced its structure and surface chemistry. Lignin fractions obtained using DGDE:ET + PTSA, ET + PTSA and NaOH (L-DGDE:ET + PTSA, L-ET + PTSA and L-NaOH) were compared with lignin isolated using the classical Klason method (L-Klason).

FTIR spectra (Figure 7b−c) showed that all solvent-derived lignins preserved the characteristic lignin fingerprint but exhibited clear modifications relative to L-Klason. In the high-frequency region (Figure 7b), the O−H stretching band appeared broader in L-NaOH, L-ET + PTSA and L-DGDE:ET + PTSA, whereas L-Klason displayed a sharper profile. This behavior is consistent with partial overlap from N−H vibrations reported for amine-containing lignins.[79] A distinctive band at 1708 cm^{-1}, assigned to C═O stretching in oxidized lignin structures,[39,40] was observed in L-Klason but was absent or strongly suppressed in solvent-derived lignins. In the fingerprint region (Figure 7c), all samples displayed aromatic C═C and C−H bands together with C−O vibrations typical of lignin.[57,58] Solvent-treated lignins additionally showed features associated with residual carbohydrates, including C−O−C and C−H deformations,[45] which were minimal or absent in L-Klason. Weak bands compatible with S═O and N−H vibrations were also present in ET- and DGDE:ET-derived lignins, in agreement with previous assignments for sulfonated and aminated lignins.[55,80] Residual hemicellulose markers (~1200, 1040, and 900 cm^{-1}) were more pronounced in these lignins than in L-Klason, confirming coprecipitation of small amounts of carbohydrate residues.[39,40] Spectra from SGB-C lignins (Figure S21) exhibited the same band families but with more pronounced intensity variations,

https://doi.org/10.1021/acssuschemeng.6c00062
ACS Sustainable Chem. Eng. XXXX, XXX, XXX−XXX

reflecting the greater recalcitrance of rind-containing biomass.[59]

SEM images (Figure 8) showed that all lignins formed irregular aggregated blocks with fractured and rough surfaces,

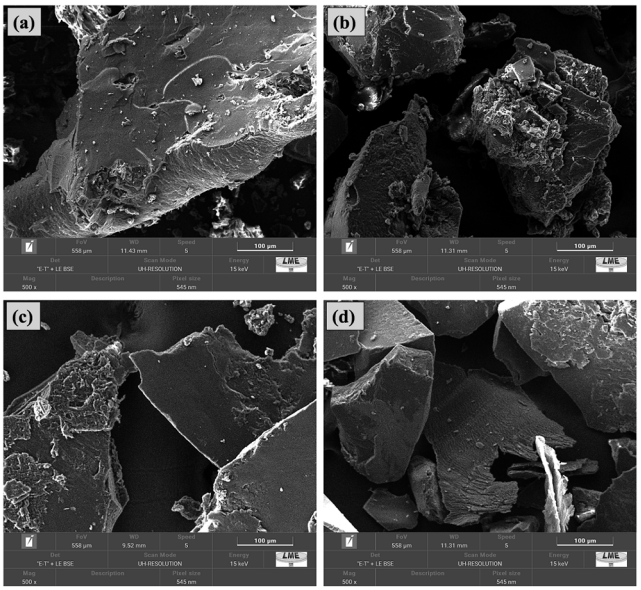

Figure 8. SEM images of lignins from SGB: (a) L-Klason; (b) L-DGDE:ET + PTSA; (c) L-ET + PTSA; and (d) L-NaOH. L-X (X = solvent or extraction method) represents the lignin fractions.

markedly distinct from the lamellar morphology of the holocellulosic fractions. L-Klason appeared as compact and brittle blocks, characteristic of lignins obtained under strong acid hydrolysis.[81] L-DGDE:ET + PTSA and L-ET + PTSA displayed more extensive fragmentation, higher surface roughness and fine adhered debris, consistent with reprecipitation-driven fracturing phenomena previously reported in the literature.[82,83] In contrast, L-NaOH formed comparatively more cohesive particles with fewer fractures. Lignins obtained from SGB-C (Figure S24) showed similar morphological patterns across treatments, indicating consistent aggregation behavior independent of rind.[82]

According to the EDS analysis (Tables S12−S13), L-Klason exhibited markedly different O/S ratios depending on the biomass. For SGB, oxygen and sulfur accounted for 63.94% and 36.06%, respectively. In SGB-C the proportions shifted to 91.67% of oxygen and 8.33% of sulfur, indicating lower residual sulfur and higher density of oxygenated groups in rind-containing bagasse. L-DGDE:ET + PTSA and L-ET + PTSA contained oxygen together with substantial nitrogen and lower levels of sulfur, reflecting incorporation of amine- and sulfonate-derived functionalities.[80,84,85] NaOH-derived lignin was dominated by oxygen, with detectable sodium and silicon originating from counterions and mineral residues.[33] Although these elemental contents were consistent between SGB and SGB-C, SGB-C-derived lignins showed comparatively higher sulfur content in ET- and DGDE:ET solvents, in agreement with the FTIR evidence of S-containing groups.[55]

Corroborating the EDS results, CHNS elemental analysis (Table S14) revealed significant differences in the composition of the recovered lignins. For SGB, the lignin obtained by the Klason method exhibited a high carbon content (53.5%) and low nitrogen (0.5%) and sulfur (0.8%) levels, consistent with a more aromatic and less functionalized structure. L-DGDE:ET + PTSA showed a reduced carbon content (45.6%) accompanied by a substantial increase in nitrogen (3.71%) and sulfur (1.7%), while L-ET + PTSA presented 44.2% C, 3.66% N, and 1.9% S.

For SGB-C, higher carbon contents were observed for L-Klason (55.3%) and L-DGDE:ET + PTSA (49.3%), with even higher nitrogen (up to 4.08%) and sulfur (1.44%) contents in DES-derived lignin. L-ET + PTSA exhibited 46.6% C, 2.8% N, and 0.7% S. L-NaOH was characterized by 45.7% C, sulfur content of 0.05%, and a higher oxygen fraction (47.9%), evidencing the absence of significant sulfur incorporation typically associated with acid-mediated fractionation. Compared to SGB, lignins derived from SGB-C consistently showed higher carbon contents and greater retention of N and S in DES-treated samples, suggesting stronger solvent−biomass interactions in the presence of rind-containing material.

To further assess structural modifications, the atomic H/C and O/C ratios were calculated from CHNS elemental analysis. For SGB-derived lignins, L-Klason exhibited the lowest H/C (1.07) and O/C (0.57) ratios, consistent with a more condensed and aromatic structure. In contrast, L-DGDE:ET + PTSA and L-ET + PTSAshowed markedly higher H/C (1.58−1.71) and O/C (0.88−0.93) ratios, indicative of increased aliphatic character and oxygen enrichment.

A similar trend was observed for SGB-C samples. L-Klason again displayed the lowest H/C (1.05) and O/C (0.52), while L-DGDE:ET + PTSA and L-ET + PTSA presented higher H/C (1.53−1.65) and O/C (0.59−0.70) ratios. L-NaOH showed H/C of 1.52 and O/C of 0.79, suggesting partial oxidation or increased hydroxyl content relative to L-Klason.

The systematic shift of L-DGDE:ET + PTSA and L-ET + PTSA toward higher H/C and O/C ratios indicates increased functionalization and reduced aromatic condensation compared to Klason lignin. However, elemental analysis alone does not allow discrimination between covalent structural modification and partial coprecipitation or residual association of solvent-derived components.

Complementary ^{1}H NMR analysis (Figure S22) provides additional structural insight supporting the elemental trends. The L-Klason lignin exhibited a spectral profile typical of highly condensed material, with a stronger relative contribution in the aromatic region (≈6.2−7.8 ppm) and less defined signals in the β-O-4 region (≈4.5−5.0 ppm), consistent with extensive acid-induced cleavage and subsequent C−C condensation reactions. In contrast, DGDE:ET + PTSA and ET + PTSA-derived lignins showed increased intensity and complexity in the 3.0−4.0 ppm region, attributable to overlapping lignin methoxyl signals and resonances associated with ethoxylated fragments and/or residual ethanolamine moieties. This enhanced aliphatic signal contribution is in agreement with the higher H/C ratios observed by elemental analysis and supports a lower degree of aromatic condensation together with greater preservation and/or functionalization of aliphatic side chains.

To gain deeper insight into the structural differences between L-DGDE:ET + PTSA and L-ET + PTSA, ^{31}P NMR analysis was performed to quantitatively evaluate the distribution of hydroxyl functionalities (Figure S23). The results indicate no clear evidence of additional qualitative functionalization promoted by the second DES component. The differences observed between ET and DGDE:ET systems

https://doi.org/10.1021/acssuschemeng.6c00062
ACS Sustainable Chem. Eng. XXXX, XXX, XXX−XXX

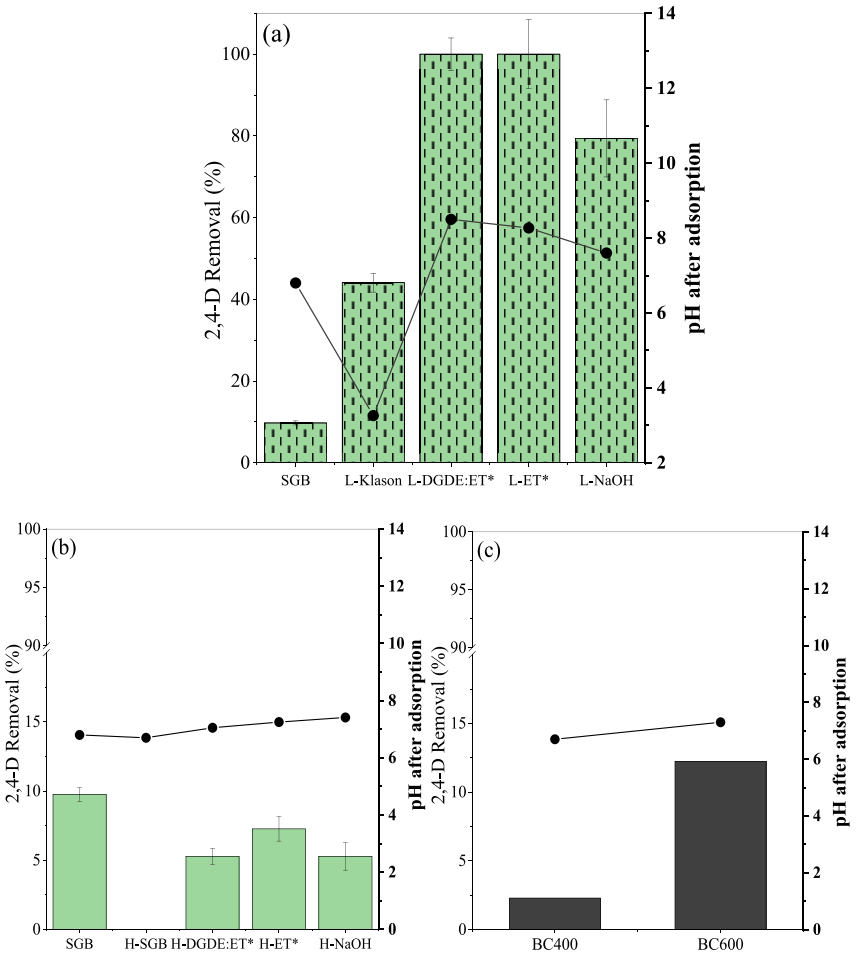

Figure 9. (a) 2,4-D removal by SGB and recovered lignins (bars); (b) 2,4-D removal by SGB and holocellulosic fractions (bars) and (c) 2,4-D removal by biochars (BC400, BC600) from previous studies (bars). L-X represents the lignin fractions, while H-X denotes the holocellulose fractions obtained after delignification, including the holocellulose sample from original bagasse (X = solvent used in the treatment or the bagasse). Dots show pH after adsorption. Values are mean ± SD. Adsorption conditions: [2,4-D] = 10 mg L^{-1}, initial pH 6.00, dose of 2 g L^{-1}, 24 h, 120 rpm, and 25 °C. *Addition of PTSA.

are essentially quantitative rather than qualitative in terms of hydroxyl-type distribution (Table S15). This finding supports the interpretation that diethylene glycol dimethyl ether primarily acts as a physical solubilization medium, whereas ethanolamine is the main reactive agent responsible for nitrogen incorporation and the increased functionalization reflected in the CHNS data and the elevated H/C and O/C ratios.

Overall, solvent-precipitated lignins differed markedly from L-Klason in both structure and surface chemistry, displaying signatures of residual carbohydrates and O, N and S functionalization. These heteroatoms, introduced either through solvent-lignin interactions or during precipitation, significantly modify the polarity and reactivity of the lignin surface,[86,87] expanding their potential for adsorption-based applications.

TGA analyses of lignins obtained using different solvents revealed marked differences in thermal stability (Figure S25). L-Klason showed the typical behavior of a highly condensed structure, with broad thermal degradation and 31% of residue after 700 °C. L-DGDE:ET + PTSA exhibited the largest degradation peak (≈460 °C) and a residue comparable to L-Klason, indicating strong condensation. In contrast, L-ET + PTSA showed a smaller degradation temperature range and a higher residue (33%), suggesting lower stability and possible carbohydrate coprecipitation. L-NaOH showed the lowest residue (23%) and degradation below 400 °C, characteristic of less condensed, more depolymerized materials. Lignins recovered from SGB-C (Figure S26) displayed similar trends but with higher residues (26−40%) and lower degradation temperatures, indicating even more recalcitrant structures likely associated with rind-derived aromatic compactness.

Together, these structural, chemical and thermal features demonstrate that solvent-driven lignin recovery not only alters the degree of condensation and functionalization but also generates materials with distinct reactivity profiles, reinforcing the critical role of solvent choice in tailoring lignin properties for downstream applications.

3.5.3. Herbicide Removal Potential. In addition to generating a holocellulosic solid fraction, this work sought to valorize the underutilized biorefinery residue rich in lignin and delignification byproducts by applying it as a biosorbent for the removal of the herbicide 2,4-D from aqueous media. Adsorption tests were performed at 10 mg L^{-1} of 2,4-D, a deliberately challenging concentration since this herbicide typically occurs in natural waters at μg L^{-1} levels.[88] Using such a higher concentration enables the assessment of adsorbent performance under critical contamination scenarios, such as

https://doi.org/10.1021/acssuschemeng.6c00062
ACS Sustainable Chem. Eng. XXXX, XXX, XXX−XXX

spills or accidental releases, while also imposing stricter operational conditions.

Clear differences were observed among the tested samples (Figure 9). Raw SGB exhibited low removal (~9.8%), confirming that the intact lignocellulosic structure provides limited interaction with 2,4-D. L-Klason achieved ~44% removal, highlighting the relevance of phenolic and aromatic units, whose electron-rich π-domains enable $\pi-\pi$ stacking with the herbicide's aromatic ring.[89,90]

The lignins recovered using alternative solvents performed remarkably well. L-DGDE:ET + PTSA and L-ET + PTSA achieved complete removal (100%) of 2,4-D, whereas L-NaOH reached only 79.4%. Beyond aromaticity, the amination and sulfonation identified in L-DGDE:ET + PTSA and L-ET + PTSA likely increased the density of functional groups interacting with ionizable pollutants, yielding performance far superior to conventional lignin and to unmodified biochars.

Solution pH after adsorption supported these interpretations. L-Klason acidified the medium to pH 3.3, while L-DGDE:ET + PTSA and L-ET + PTSA resulted in alkaline final pH values (8.3−8.5). L-NaOH remained near neutral (7.6). This is particularly relevant because many studies report efficient 2,4-D adsorption only under highly acidic conditions (pH 2−3).[91,92] In contrast, the lignins obtained in this work performed effectively at an initial pH of 6, which is much closer to natural aquatic environments.

On the other hand, holocellulosic fractions displayed poor adsorption (0−7.3%), consistent with its higher polarity, and the absence of aromatic or carboxylic groups. Unmodified biochars (BC400 and BC600) also performed poorly (2.3% and 12.2%), in line with literature reports indicating that pristine biochars typically require chemical modification to reach competitive adsorption levels[9,34] Qualitatively, the removals observed for L-DGDE:ET + PTSA and L-ET + PTSA are comparable to or higher than the efficiencies often reported for lignin- or biochar-based adsorbents produced through chemical activation or surface modification, reinforcing the high intrinsic functionality of the recovered lignins.

Overall, the results show that lignin recovered through alternative routes is not merely a coproduct but a highly functional biosorbent with superior performance under environmentally relevant conditions. The combination of preserved aromaticity, enhanced surface chemistry and favorable pH interactions positions these materials as effective candidates for the remediation of phenoxyacetic herbicides such as 2,4-D.

3.6. Evaluation of Fractionation Performance and Process Sustainability

Conventionally, selectivity in lignocellulosic fractionation is expressed as the ratio between lignin removal and holocellulose loss.[93] However, in the present study, the differences in holocellulose mass before and after treatment with DGDE:ET + PTSA, ET + PTSA, or 3% (m/v) NaOH were within the experimental uncertainty of the gravimetric measurements (<0.002 g), indicating negligible solubilization of the carbohydrate fraction. These results confirm satisfactory mass-balance closure for holocellulose throughout the process and demonstrate the high selectivity of the evaluated solvents toward lignin removal under the tested conditions.

Under these circumstances, the conventional selectivity ratio becomes inadequate for comparing solvent performance, since holocellulose loss approaches zero, resulting in artificially inflated or undefined values. To enable a quantitative and consistent comparison among solvent systems, a comparative index (CI) was defined as the ratio between the percentage of precipitated lignin recovered in the final recovery step (with Klason lignin taken as the 100% reference) and the degree of holocellulose not preserved in the treated solid fraction, as expressed in eq 6:

$$CI = \frac{Precipitated\ lignin(\%)}{100 - Holocellulose(\%)} \quad (6)$$

Given the high degree of holocellulose preservation observed, CI becomes mathematically sensitive to small variations in carbohydrate content. Therefore, while CI provides a useful comparative tool under near-zero carbohydrate loss conditions, it should not be interpreted as an absolute selectivity descriptor.

The calculated values are presented in Table S15. For SGB, ET + PTSA exhibited the highest CI (9.60; 56.0% precipitated lignin and 94.17% holocellulose), followed by DGDE:ET + PTSA (CI = 4.75; 51.0% lignin and 89.26% holocellulose), both outperforming 3% NaOH (CI = 3.21; 40.95% lignin and 87.25% holocellulose). For SGB-C, CI values were lower overall. 3% NaOH showed the highest CI (3.85), whereas ET + PTSA (CI = 2.71) and DGDE:ET + PTSA (CI = 2.33) maintained high holocellulose contents (>84%), indicating effective carbohydrate preservation.

Overall, while ET + PTSA exhibited the highest CI for SGB and NaOH showed higher CI values for SGB-C, DGDE:ET + PTSA demonstrated consistently high holocellulose preservation combined with substantial lignin recovery under milder operating conditions. Therefore, its selection is supported not only by the comparative index but also by its balanced fractionation performance within the integrated process framework adopted in this study.

Other important aspects must be considered to properly assess process sustainability. Although the precipitation strategy adopted in this work for lignin recovery, comprising dilution of the DES extract with water, acidification with H_2SO_4, and successive concentration/redispersion cycles (Section 2.6 and Figure 6b), proved effective in maximizing lignin recovery, it raises important considerations from a sustainability and process engineering standpoint, particularly regarding solvent recyclability and overall mass balance.

Partial evaporation was conducted at 60 °C; however, complete water removal is unlikely under such mild conditions. Progressive water accumulation may therefore modify solvent polarity, effective acidity, viscosity, and hydrogen-bond donor−acceptor interactions, potentially affecting extraction performance in subsequent reuse cycles. In addition, acidification with H_2SO_4 introduces a second strong acid into the DES+PTSA medium, which may alter the original eutectic equilibrium through proton exchange and ionic redistribution.

The elevated nitrogen and sulfur contents observed in DES-derived lignins (Section 3.5.2) indicate that solvent components are not fully recovered and may remain strongly associated with, or partially incorporated into, the lignin fraction. Such retention directly impacts solvent recovery efficiency and may progressively shift DES composition during recycling. Furthermore, not all solubilized lignin necessarily precipitates under the applied dilution and acidification conditions, as reflected by the yields of precipitated lignin (Table S14). A fraction of lower-molecular-weight or highly

https://doi.org/10.1021/acssuschemeng.6c00062
ACS Sustainable Chem. Eng. XXXX, XXX, XXX−XXX

functionalized lignin fragments may remain soluble in the recovered solvent phase. From a process perspective, the persistence of soluble lignin in the recycled solvent stream may lead to gradual accumulation of aromatic species, potentially altering solvent physicochemical properties and extraction selectivity over multiple cycles. Conversely, this soluble fraction may represent a selectively depolymerized lignin stream with distinct chemical functionality, offering opportunities for targeted valorization. A comprehensive assessment of soluble lignin content and its evolution during solvent recycling is therefore necessary to establish a complete mass balance and long-term process stability

4. CONCLUSION AND FUTURE PERSPECTIVES

This work demonstrates that DES fractionation, supported by rational solvent selection and systematic experimental optimization, enables mild and selective delignification of sugar cane bagasse while allowing the concurrent recovery of high-purity holocellulose and chemically functionalized lignin. The DES composed of diethylene glycol dimethyl ether and ethanolamine (DGDE:ET), acidified with PTSA, promoted extensive lignin removal under mild conditions (DGDE molar fraction 0.10, 100 °C, 0.03 mol L^{-1} PTSA, 90 min, S/L = 1:10) and generated holocellulose-rich solids containing 88.9 ± 2.6% holocellulose for rind-free bagasse (SGB), performing comparably to or surpassing alkaline pretreatment (3% w v^{-1} NaOH) while avoiding its corrosive nature and additional purification steps. The DES also remained effective for rind-containing bagasse (SGB-C), although its higher recalcitrance and high extractives and mineral content reduced delignification efficiency relative to SGB.

Recovered lignins from both SGB and SGB-C displayed clear O/N/S functionalization and achieved 100% removal of 2,4-dichlorophenoxyacetic acid (2,4-D) at near-neutral pH, surpassing alkaline lignin (79.4%), Klason lignin (approximately 44%), holocellulosic fractions (0−7.3%), original bagasse (approximately 9.8%) and biochars (2.3% for BC400 and 12.2% for BC600). Although lignin precipitation from DES posed operational challenges, mainly due to strong buffering and low lignin content, the recovered materials exhibited high functional potential for environmental remediation. Holocellulose-rich fractions retained high structural integrity and exhibited negligible adsorption, supporting their suitability for conversion into higher-value products.

These outcomes also highlight the value of COSMO-RS as a predictive tool for solvent selection, enabling the rational identification of DES with high affinity for lignin prior to experimental validation and significantly reducing experimental screening efforts. While systematic multicycle recycling studies combined with detailed compositional analysis are necessary to fully establish long-term solvent stability and overall process sustainability, this study shows that DES fractionation enables integrated recovery of structurally preserved holocellulose and highly functionalized lignin from both SGB and SGB-C. These findings support the potential of DES as versatile and more sustainable solvents for advancing efficient, selective, and circular biorefinery strategies.

■ ASSOCIATED CONTENT

Data Availability Statement

Data available on request due to privacy/ethical restrictions

Supporting Information

The Supporting Information is available free of charge at https://pubs.acs.org/doi/10.1021/acssuschemeng.6c00062.

DES components and formation (Tables S1−S2); response surface methodology design and statistical analysis (Tables S3−S4, S7−S11); additional optimization data (Tables S8−S10); compositional analysis (Table S5); FTIR band assignments (Table S6); CHNS, NMR, and EDS elemental analysis (Tables S12−S15); comparative index data (Table S16); COSMO-RS screening results (Figure S4); additional FTIR, SEM, and TGA/DTG characterization of raw materials, holocellulosic fractions, lignins, solvents, and intermediate fractions (Figures S1−S3, S5−S26) (PDF)

■ AUTHOR INFORMATION

Corresponding Authors

Ana M. Ferreira − *CICECO, Aveiro Institute of Materials, Department of Chemistry, University of Aveiro, Aveiro 3810-193, Portugal;* orcid.org/0000-0003-3057-5019; Email: ana.conceicao@ua.pt

Filipe H. B. Sosa − *CICECO, Aveiro Institute of Materials, Department of Chemistry, University of Aveiro, Aveiro 3810-193, Portugal*; Email: filipesosa@ua.pt

Guilherme M. D. Ferreira − *Group of Materials, Interfaces, and Solutions (MatIS), Department of Chemistry, Federal University of Lavras, Lavras, Minas Gerais 37200-900, Brazil;* orcid.org/0000-0002-4762-2777; Email: guilherme.ferreira@ufla.br

Authors

Thamiris F. Souza − *Group of Materials, Interfaces, and Solutions (MatIS), Department of Chemistry, Federal University of Lavras, Lavras, Minas Gerais 37200-900, Brazil;* orcid.org/0000-0001-6775-6767

João A. P. Coutinho − *CICECO, Aveiro Institute of Materials, Department of Chemistry, University of Aveiro, Aveiro 3810-193, Portugal;* orcid.org/0000-0002-3841-743X

Cecília B. Ferreira − *Group of Materials, Interfaces, and Solutions (MatIS), Department of Chemistry, Federal University of Lavras, Lavras, Minas Gerais 37200-900, Brazil*

Complete contact information is available at: https://pubs.acs.org/10.1021/acssuschemeng.6c00062

Funding

The Article Processing Charge for the publication of this research was funded by the Coordenacao de Aperfeicoamento de Pessoal de Nivel Superior (CAPES), Brazil (ROR identifier: 00x0ma614).

Notes

Declaration of Generative AI and AI-assisted technologies in the writing process: During the preparation of this work, the authors used ChatGPT to refine the language and clarity of the manuscript. The authors reviewed and edited the content as needed and take full responsibility for the content of the publication.

The authors declare no competing financial interest.

■ ACKNOWLEDGMENTS

This work was partly developed within the scope of the project CICECO Aveiro Institute of Materials, UID/50011/2025 (DOI: 10.54499/UID/50011/2025) & LA/P/0006/2020 (DOI: 10.54499/LA/P/0006/2020), financed by national funds through the FCT/MCTES (PIDDAC). This work is also funded by national funds through FCT − Fundação para a Ciência e a Tecnologia, I.P., under the project GREEN-PATH (ref. 2023.15169.PEX, DOI: 10.54499/2023.15169.PEX). AMF and FHBS acknowledge FCT for the research contracts CEECIND/00361/2022 (DOI: 10.54499/2022.00361.CEECIND/CP1720/CT002) and CEECIND/07209/2022, respectively. The authors are grateful for the financial support of the agencies CNPq (406474/2021-4; 407799/2022-2) and FAPEMIG (APQ-04229-23; RED-00161-23). This study was financed in part by the Coordenação de Aperfeiçoamento de Pessoal de Nível Superior − Brazil (CAPES), under the PhD Sandwich Program (PDSE), Finance Code 001 (Process No. 88881.981986/2024-01). Additional support was provided by FAPEMIG (doctoral scholarship granted to T. F. Souza) and by CNPq (fellowship granted to G. M. D. Ferreira − Grant No. 309999/2022-7). The authors are also grateful to the Center for Chemical Analysis and Prospection (CAPQ) of the Federal University of Lavras (UFLA) for providing the equipment and technical support for experiments involving FTIR and TGA; to the Laboratory of Electron Microscopy and Ultrastructural Analysis (LME) in the Department of Plant Pathology, UFLA, for providing the equipment for SEM and EDS analyses; FINEP, FAPEMIG, CNPq, and CAPES for funding these laboratories. The authors also acknowledge the Laboratory of Professor Fabio Akira Mori (UFLA) for assistance with extractives determination and Professor Victor Freitas (UFSJ) for performing the FTIR analyses.

■ REFERENCES

(1) de Almeida, S. G. C.; et al. Biochar production from sugarcane biomass using slow pyrolysis: Characterization of the solid fraction. *Chem. Eng. Process.: Process Intensif.* **2022**, *179*, 109054.
(2) FAO. *Crops and Livestock Products*. 2025 https://www.fao.org/faostat/en/#data/QCL/visualize.
(3) Ajala, E. O.; Ighalo, J. O.; Ajala, M. A.; Adeniyi, A. G.; Ayanshola, A. M.; et al. Sugarcane bagasse: a biomass sufficiently applied for improving global energy, environment and economic sustainability. *Bioresour. Bioprocess* **2021**, *8* (1), 87.
(4) Tantayotai, P.; et al. In-depth investigation of the bioethanol and biogas production from organic and mineral acid pretreated sugarcane bagasse: Comparative and optimization studies. *Biocatal. Agric. Biotechnol* **2022**, *45*, 102499.
(5) Ramlee, N. A.; Naveen, J.; Jawaid, M. Potential of oil palm empty fruit bunch (OPEFB) and sugarcane bagasse fibers for thermal insulation application−A review. *Constr. Build. Mater* **2021**, *271*, 121519.
(6) An, Q.; et al. Biological saccharification by Clostridium thermocellum and two-stage hydrogen and methane production from hydrogen peroxide-acetic acid pretreated sugarcane bagasse. *Int. J. Hydrogen Energy* **2020**, *45* (55), 30211−30221.
(7) de Paiva, F. F. G.; et al. Sugarcane bagasse fiber as semi-reinforcement filler in natural rubber composite sandals. *J. Mater. Cycles Waste Manage* **2019**, *21* (2), 326−335.
(8) Gupta, H.; et al. Synthesis of biodegradable films obtained from rice husk and sugarcane bagasse to be used as food packaging material. *Environ. Eng. Res* **2020**, *25* (4), 506−514.
(9) Souza, T. F.; et al. Influence of Mn precursor on pre-pyrolysis modification of sugarcane bagasse biochar for enhanced removal of 2,4-dichlorophenoxyacetic acid from aqueous solutions: Experimental and theoretical insights. *J. Environ. Chem. Eng* **2024**, *12* (5), 113499.
(10) Aigaje, E.; Riofrio, A.; Baykara, H. Processing, properties, modifications, and environmental impact of nanocellulose/biopolymer composites: a review. *Polymers* **2023**, *15* (5), 1219.
(11) Del Valle, L. J.; Díaz, A.; Puiggalí, J. Hydrogels for biomedical applications: cellulose, chitosan, and protein/peptide derivatives. *Gels* **2017**, *3* (3), 27.
(12) Marinho, E. Cellulose: A comprehensive review of its properties and applications. *Sustainable Chem. Environ* **2025**, *11*, 100283.
(13) Takkellapati, S.; Li, T.; Gonzalez, M. A. An overview of biorefinery-derived platform chemicals from a cellulose and hemicellulose biorefinery. Clean technologies and environmental policy. *Clean Technol. Environ. Policy* **2018**, *20* (7), 1615−1630.
(14) Liu, Y.; et al. Process optimization for deep eutectic solvent pretreatment and enzymatic hydrolysis of sugar cane bagasse for cellulosic ethanol fermentation. *Renewable Energy* **2021**, *177*, 259−267.
(15) Ragauskas, A. J.; Williams, C. K.; Davison, B. H.; Britovsek, G.; Cairney, J.; Eckert, C. A.; Frederick, W. J., Jr.; Hallett, J. P.; Leak, D. J.; Liotta, C. L.; et al. The path forward for biofuels and biomaterials. *Science* **2006**, *311* (5760), 484−489.
(16) Sun, Y.; et al. Facile synthesis of Fe-modified lignin-based biochar for ultra-fast adsorption of methylene blue: Selective adsorption and mechanism studies. *Bioresour. Technol* **2022**, *344*, 126186.
(17) Mel, M.; Lau, B.; Hockaday, W. C. Sorption of per- and polyfluoroalkyl substances by lignin in pulp and paper wastewater. *J. Hazard. Mater* **2024**, *480*, 136016.
(18) Yin, X.; et al. The pretreatment of lignocelluloses with green solvent as biorefinery preprocess: a minor review. *Front. Plant Sci* **2021**, *12*, 670061.
(19) Martins, M. A. R.; Pinho, S. P.; Coutinho, J. A. P. Insights into the nature of eutectic and deep eutectic mixtures. *J. Solution Chem* **2019**, *48*, 962−982.
(20) Prabhune, A.; Dey, R. Green and sustainable solvents of the future: Deep eutectic solvents. *J. Mol. Liq* **2023**, *379*, 121676.
(21) Morán-Aguilar, M. G.; et al. Development of sustainable biorefinery processes applying deep eutectic solvents to agrofood wastes. *Energies* **2022**, *15* (11), 4101.
(22) Valladares-Diestra, K. K.; et al. Integrated sugarcane biorefinery for first- and second-generation bioethanol production using imidazole pretreatment. *J. Clean. Prod* **2022**, *381*, 135179.
(23) Chourasia, V. R.; et al. Improving enzymatic digestibility of sugarcane bagasse from different varieties of sugarcane using deep eutectic solvent pretreatment. *Bioresour. Technol* **2021**, *337*, 125480.
(24) Varilla-Mazaba, A.; Raggazo-Sánchez, J. A.; Calderón-Santoyo, M.; Gómez-Rodríguez, J.; Aguilar-Uscanga, M. G.; et al. Optimization of lignin extraction by response surface methodology from sugarcane bagasse using deep eutectic solvents (DES). Industrial Crops and Products. *Ind. Crops Prod* **2022**, *184*, 115040.
(25) Li, B.; et al. Application of Aromatic Ring Quaternary Ammonium and Phosphonium Salts−Carboxylic Acids-Based Deep Eutectic Solvent for Enhanced Sugarcane Bagasse Pretreatment, Enzymatic Hydrolysis, and Cellulosic Ethanol Production. *Fermentation* **2023**, *9* (11), 981.
(26) Sunar, S. L.; et al. Deep eutectic solvent pretreatment of sugarcane bagasse for efficient lignin recovery and enhanced enzymatic hydrolysis. *J. Ind. Eng. Chem* **2024**, *139*, 539−553.
(27) Xian, X.; Li, B.; Feng, S.; Huang, J.; Fu, X.; Wu, T.; Lin, X.; et al. Enhanced bioethanol production from sugarcane bagasse: combination of liquid hot water and deep eutectic solvent pretreatment for optimized enzymatic saccharification. *Front. Chem. Sci. Eng* **2024**, *18* (8), 85.
(28) Wojeicchowski, J. P.; et al. Using COSMO-RS in the Design of Deep Eutectic Solvents for the Extraction of Antioxidants from Rosemary. *ACS Sustainable Chem. Eng* **2020**, *8* (32), 12132−12141.

(29) Pontes, P. V. A.; et al. COSMO-RS assisted selection of eutectic solvents for lignin dissolution and enhanced laccase activity. *Int. J. Biol. Macromol* **2025**, *320*, 146048.
(30) del Río, J. C.; et al. Differences in the chemical structure of the lignins from sugarcane bagasse and straw. *Biomass Bioenergy* **2015**, *81*, 322−338.
(31) Alvarez-Vasco, C.; et al. Unique low-molecular-weight lignin with high purity extracted from wood by deep eutectic solvents (DES): a source of lignin for valorization. *Green Chem* **2016**, *18* (19), 5133−5141.
(32) Soares, B.; et al. Wood delignification with aqueous solutions of deep eutectic solvents. *Ind. Crops Prod* **2021**, *160*, 113128.
(33) Nguyen-Thi, N. Y.; et al. Extracting lignin from sugarcane bagasse for methylene blue and hexavalent chromium adsorption in textile wastewater: a facile, green, and sustainable approach††Electronic supplementary information (ESI) available. *RSC Adv* **2024**, *14* (7), 4533−4542.
(34) Souza, T. F.; Lobato, R. L. M.; Maia, L. C.; Louzada, L. N.; Faria, M. E. A.; Fernandes, L. F.; Gurgel, L. V. A.; Ferreira, G. M. D.; Ribeiro−Soares, J.; Ferreira, G. M. D. Biochar-Iron Oxide Composites for Adsorption of Chlorophenoxy Herbicides: Impact of Chlorine Substituents on Bath and Continuous Adsorption Performance. *Adv. Sustainable Syst* **2025**, *9*, No. e00628.
(35) Frankó, B.; et al. Removal of water-soluble extractives improves the enzymatic digestibility of steam-pretreated softwood barks. *Appl. Biochem. Biotechnol* **2018**, *184* (2), 599−615.
(36) Lee, S. C.; Mariatti, M. The effect of bagasse fibers obtained (from rind and pith component) on the properties of unsaturated polyester composites. *Mater. Lett* **2008**, *62* (15), 2253−2256.
(37) Zoghlami, A.; Paës, G. Lignocellulosic biomass: understanding recalcitrance and predicting hydrolysis. *Front. Chem* **2019**, *7*, 874.
(38) Mondal, S.; Neogi, S.; Chakraborty, S. Experimental and kinetic analyses of delignification of lignocellulosic grass with minimal holocellulose loss during pretreatment. *Bioresour. Technol. Rep* **2023**, *23*, 101549.
(39) Lu, H.; et al. Efficient delignification of sugarcane bagasse by Fenton oxidation coupled with ultrasound-assisted NaOH for biotransformation from Agaricus sinodeliciosus var. Chaidam. *Chem. Eng. J* **2022**, *448*, 137719.
(40) Yoon, L. W.; et al. Comparison of ionic liquid, acid and alkali pretreatments for sugarcane bagasse enzymatic saccharification. *J. Chem. Technol. Biotechnol* **2011**, *86* (10), 1342−1348.
(41) Oh, S. Y.; et al. FTIR analysis of cellulose treated with sodium hydroxide and carbon dioxide. *Carbohydr. Res* **2005**, *340* (3), 417−428.
(42) Via, B. K.; Fasina, O.; Pan, H. Assessment of pine biomass density through mid-infrared spectroscopy and multivariate modeling. *BioResources* **2013**, *6*, 807−822.
(43) Dwivedi, E.; Singh, L. K. Characterization of lignin from sugarcane bagasse by Raman spectroscopy and FTIR. *Int. J. Health Sci* **2022**, *6*, 12260−12268.
(44) Lan, W.; Liu, C.-F.; Sun, R.-C. Fractionation of bagasse into cellulose, hemicelluloses, and lignin with ionic liquid treatment followed by alkaline extraction. *J. Agric. Food Chem* **2011**, *59* (16), 8691−8701.
(45) Pimentel, L. G.; et al. Diffuse Reflectance Infrared Fourier Transform (DRIFT) spectroscopy to assess decomposition dynamics of sugarcane straw. *Bioenergy Res* **2019**, *12*, 909−919.
(46) Mohomane, S. M.; Motaung, T. E.; Revaprasadu, N. Thermal degradation kinetics of sugarcane bagasse and soft wood cellulose. *Materials* **2017**, *10* (11), 1246.
(47) Canettieri, E. V.; da Silva, V. P.; Neto, T. G. S.; Hernández-Pérez, A. F.; da Silva, D. D. V.; Dussán, K. J.; das Graças Almeida Felipe, M.; de Carvalho, J. A., Jr.; et al. Physicochemical and thermal characteristics of sugarcane straw and its cellulignin. *J. Braz. Soc. Mech. Sci. Eng* **2018**, *40* (9), 416.
(48) Escalante, J.; et al. Pyrolysis of lignocellulosic, algal, plastic, and other biomass wastes for biofuel production and circular bioeconomy: A review of thermogravimetric analysis (TGA) approach. *Renewable Sustainable Energy Rev* **2022**, *169*, 112914.
(49) Lu, X.; Gu, X. A review on lignin pyrolysis: pyrolytic behavior, mechanism, and relevant upgrading for improving process efficiency. *Biotechnol. Biofuels Bioprod* **2022**, *15* (1), 106.
(50) Arul Mozhi Selvan, V.; Kumar, M. H. Experimental and Statistical Analysis on Thermo-mechanical properties of Sodium Chloride and Alkaline Treated Sugarcane Bagasse Fiber Thermo-mechanical properties of sodium chloride and alkali-treated sugarcane bagasse fibre. *Indian J. Fibre Text. Res.* **2018**.
(51) Goldstein, J. I.; Newbury, D. E.; Michael, J. R.; Ritchie, N. W.; Scott, J. H. J.; Joy, D. C. *Scanning electron microscopy and X-ray microanalysis*. Springer, 2018.
(52) Zubeltzu, J.; Formoso, E.; Rezabal, E. Lignin solvation by ionic liquids: The role of cation. *J. Mol. Liq* **2020**, *303*, 112588.
(53) Vigier, K. D. O.; Chatel, G.; Jérôme, F. Contribution of deep eutectic solvents for biomass processing: opportunities, challenges, and limitations. *ChemCatChem* **2015**, *7* (8), 1250−1260.
(54) Francisco, M.; Van Den Bruinhorst, A.; Kroon, M. C. New natural and renewable low transition temperature mixtures (LTTMs): screening as solvents for lignocellulosic biomass processing. *Green Chem* **2012**, *14* (8), 2153−2157.
(55) Tipson, R. S. Infrared Absorption Spectra of p-Toluenesulfonic Acid and of Some of Its Esters. *J. Am. Chem. Soc* **1952**, *74* (5), 1354−1354.
(56) Jiang, Y.; et al. Liquid-liquid equilibrium data measurement and thermodynamic modelling for ternary mixtures composed of water, diethylene glycol dimethyl ether and different solvents at 298.2 K. *J. Chem. Thermodyn* **2022**, *165*, 106669.
(57) Zhao, Z.; et al. Pretreatment of wheat straw using basic ethanolamine-based deep eutectic solvents for improving enzymatic hydrolysis. *Bioresour. Technol* **2018**, *263*, 325−333.
(58) Marshall, B. D. A molecular equation of state for alcohols which includes steric hindrance in hydrogen bonding. *J. Chem. Phys* **2018**, *149* (4), 044505.
(59) Naik, P. K.; Paul, S.; Banerjee, T. Physiochemical Properties and Molecular Dynamics Simulations of Phosphonium and Ammonium Based Deep Eutectic Solvents. *J. Solution Chem* **2019**, *48* (7), 1046−1065.
(60) Fu, X.; et al. High-performance removal of methylene blue dye using porous lignin extracted from sugarcane bagasse by deep eutectic solvent. *Int. J. Biol. Macromol* **2024**, *279*, 135470.
(61) Deng, B.; et al. Kinetics of lignin separation during the atmospheric fractionation of bagasse with p-toluenesulfonic acid. *Int. J. Mol. Sci* **2022**, *23* (15), 8743.
(62) Kumar, R.; Wyman, C. E. Cellulase adsorption and relationship to features of corn stover solids produced by leading pretreatments. *Biotechnol. Bioeng* **2009**, *103* (2), 252−267.
(63) Sun, R.; Tomkinson, J. Comparative study of lignins isolated by alkali and ultrasound-assisted alkali extractions from wheat straw. *Ultrason. Sonochem* **2002**, *9* (2), 85−93.
(64) Hu, F.; Jung, S.; Ragauskas, A. Pseudo-lignin formation and its impact on enzymatic hydrolysis. *Bioresour. Technol* **2012**, *117*, 7−12.
(65) Chang, V. S.; Holtzapple, M. T. Fundamental factors affecting biomass enzymatic reactivity. *Appl. Biochem. Biotechnol.* **2000**, *84*−*86* (1), 5−37.
(66) de CM Miranda, R.; Neta, J. V.; Ferreira, L. F. R.; Júnior, W. A. G.; do Nascimento, C. S.; Gomes, E. d. B.; Mattedi, S.; Soares, C. M. F.; Lima, Á. S. Pineapple crown delignification using low-cost ionic liquid based on ethanolamine and organic acids. *Carbohydr. Polym* **2019**, *206*, 302−308.
(67) Wang, J.; et al. Pretreatment of Camellia oleifera shell by ethanolamine-based solvents for selective delignification and enhanced enzymatic saccharification. *Ind. Crops Prod* **2024**, *222*, 119523.
(68) Şen, U.; Esteves, B.; Pereira, H. Pyrolysis and extraction of bark in a biorefineries context: a critical review. *Energies* **2023**, *16* (13), 4848.

https://doi.org/10.1021/acssuschemeng.6c00062
ACS Sustainable Chem. Eng. XXXX, XXX, XXX−XXX

(69) ISO. *Colorimetry-Part 4: CIE 1976 L* a* b* colour space*; International Standard, 2007.
(70) Kumar, R.; et al. Development of a two-step hydrothermal pretreatment for sugarcane bagasse delignification surpassing acidic and chemical methods. *Waste Biomass Valorization* **2024**, *15* (8), 4613−4628.
(71) Mzimela, Z. N. T.; Linganiso, L. Z.; Revaprasadu, N.; Motaung, T. E.; et al. Comparison of cellulose extraction from sugarcane bagasse through alkali. *Mat. Res* **2018**, *21* (6), No. e20170750.
(72) Basera, P.; Chakraborty, S.; Sharma, N. Lignocellulosic biomass: insights into enzymatic hydrolysis, influential factors, and economic viability. *Discov. Sustain* **2024**, *5* (1), 311.
(73) Ao, T.-J.; et al. Influence of hemicellulose and lignin on the effect of drying of cellulose and the subsequent enzymatic hydrolysis. *Green Chem* **2025**, *27* (29), 8901−8913.
(74) Marangon Jardim, J.; Hart, P.; Lucia, L. A.; Jameel, H.; Chang, H. M. A quantitative comparison of the precipitation behavior of lignin from sweetgum and pine kraft black liquors. *BioResources* **2020**, *15* (3), 5464−5480.
(75) Ponomarev, A. V.; Vlasov, S. I.; Kholodkova, E. M. Radiation-chemical transformations of diethylene glycol dimethyl ether at room temperature and at boiling point. *Radiat. Phys. Chem* **2018**, *151*, 1−5.
(76) Wypych, A.; Wypych, G., *Databook of Solvents*. Wypych, A. A. G. ChemTec Publishing, 2014; pp. 211−281.
(77) Kienberger, M.; et al. Systematic review on isolation processes for technical lignin. *Processes* **2021**, *9* (5), 804.
(78) Chrisandina, N. J.; et al. Techno-economic analysis of water precipitation for lignin value prior to pulping. *Chem. Eng. Res. Des* **2019**, *143*, 4−10.
(79) Dai, F.; et al. Infrared spectrum characteristics and quantification of OH groups in coal. *ACS Omega* **2023**, *8* (19), 17064−17076.
(80) Sammons, R. J.; Harper, D. P.; Labbé, N.; Bozell, J.; Elder, T.; Rials, T.; et al. Characterization of organosolv lignins using thermal and FT-IR spectroscopic analysis. *BioResources* **2013**, *8* (2), 2752−2767.
(81) Geies, A.; et al. Thermal, morphological and cytotoxicity characterization of hardwood lignins isolated by in-situ sodium hydroxide-sodium bisulfate method. *Nat. Resour* **2020**, *11* (10), 427−438.
(82) Joseph, P.; Ottesen, V.; Opedal, M. T.; Moe, S. T.; et al. Morphology of lignin structures on fiber surfaces after organosolv pretreatment. *Biopolymers* **2022**, *113* (9), No. e23520.
(83) Sheridan, E.; et al. A systematic study on the processes of lignin extraction and nanodispersion to control properties and functionality. *Green Chem* **2024**, *26* (6), 2967−2984.
(84) Liu, Z.; et al. Insight into the mechanism of lignin amination pretreatment on lignin structure and its pyrolysis property for lignin valorization. *Chem. Eng. J* **2024**, *499*, 156386.
(85) Georgs, V.; et al. A critical review on lignin structure, chemistry, and modification towards utilisation in additive manufacturing of lignin-based composites. *Ind. Crops Prod* **2025**, *233*, 121416.
(86) Gordobil, O.; et al. Surface chemistry and bioactivity of colloidal particles from industrial kraft lignins. *Int. J. Biol. Macromol* **2022**, *220*, 1444−1453.
(87) Chen, J.; Liu, K.; Du, H.; Pan, X.; et al. Nitrogen-Functionalized Lignin: Current Status, Applications, and Challenges. *ChemSusChem* **2025**, *18* (16), No. e202500607.
(88) Triana Velasquez, T. M.; Bernal Bautista, M. H. Acute toxicity of the insecticide Imidacloprid and the herbicide 2, 4-D in two species of tropical anurans. *Ecotoxicology* **2025**, *34* (3), 392−400.
(89) Alluhaybi, A. A.; Alharbi, A.; Alshammari, K. F.; El-Desouky, M. G.; et al. Efficient Adsorption and Removal of the Herbicide 2, 4-Dichlorophenylacetic Acid from Aqueous Solutions Using MIL-88 (Fe)-NH2. *ACS Omega* **2023**, *8*, 40775−40784.
(90) Blachnio, M.; et al. Adsorption of phenoxyacetic herbicides from water on carbonaceous and non-carbonaceous adsorbents. *Molecules* **2023**, *28* (14), 5404.
(91) Ma, W.; et al. Pyrolyzing spent coffee ground to biochar treated with H3PO4 for the efficient removal of 2,4-dichlorophenoxyacetic acid herbicide: adsorptive behaviors and mechanism. *J. Environ. Chem. Eng* **2023**, *11* (1), 109165.
(92) Kurmysheva, A. Y.; Vedenyapina, M. D.; Kulaishin, S. A. Magnetic Activated Carbons for the Adsorption of the Typical Herbicide 2, 4-Dichlorophenoxyacetic Acid from Aquatic Media. *Solid Fuel Chem* **2022**, *56* (6), 441−447.
(93) Sun, W.; Othman, M. Z. A selective fractionation method of lignocellulosic materials using electro-assisted organosolv pretreatment. *Bioresour. Technol* **2019**, *288*, 121421.

https://doi.org/10.1021/acssuschemeng.6c00062
ACS Sustainable Chem. Eng. XXXX, XXX, XXX−XXX